Materials Today Bio 31 (2025) 101549

Contents lists available at ScienceDirect

Materials Today Bio

journal homepage: www.journals.elsevier.com/materials-today-bio

Sustained slow-release TGF-β3 in a three-dimensional-printed titanium microporous scaffold composite system promotes ligament-to-bone healing

Liwei Zhu, Yuzhe Liu, Yifu Sun, Zhenjia Che, Youbin Li, Tengyue Liu, Xudong Li, Chengzhe Yang, Lanfeng Huang *

Department of Orthopedics, The Second Hospital of Jilin University, Changchun, 130041, PR China

ARTICLE INFO

Keywords:
Tendon/ligament-to-bone healing
Transforming growth factor-β3
Bioactive interface
Titanium scaffolds
Sustained-release system

ABSTRACT

The treatment of tendon/ligament-to-bone injury is a long-standing research challenge in orthopedics and bone tissue engineering. Orderly healing of the fibrocartilage layer and mineralized bone layer is crucial for treating tendon-bone interface injuries. We designed a three-dimensional printed porous titanium scaffold composite system with thermosensitive collagen hydrogel loaded with transforming growth factor β3 (TGF-β3), formulated for the sustained slow release of TGF-β3 at a constant rate. *In vitro*, the composite system exhibited good biocompatibility and was beneficial for the adhesion and proliferation of bone marrow mesenchymal stem cells (BMSCs), which showed high growth activity. Moreover, the composite system promoted the differentiation of BMSCs via osteogenesis and chondrogenesis. *In vivo*, the composite system provided active substances at the injured site, promoting the repair of the fibrocartilage layer and of the mineralized bone layer at the interface between the ligament and bone. Micro-CT results demonstrated that the complex promotes the osseointegration of titanium scaffolds in bone defects. Hard tissue sections showed that the new bone, ligament, and the titanium alloy scaffold system formed a closely integrated whole; the composite system provided suitable attachment points for ligament growth. Additionally, the biomechanical strength of the tendon interface improved to some extent. Our results indicate that the composite system has potential as a bioactive implant interface for repairing ligament and bone injuries.

1. Introduction

The tendon/ligament-to-bone junction site is a complex structure composed of tendon/ligament, uncalcified fibrocartilage, calcified fibrocartilage, and bone [1]. It acts as an important mediator of force transmission between muscle and bone. Tendon joint injury is one of the most common diseases in the field of sports injury due to the high amount of physical stress imposed on this tissue [2]. Because of the poor regenerative properties of tendon tissue, a large amount of scar tissue is formed at the tendon-bone interface during healing and repair. Meanwhile, poor bone and the development of the fibrocartilage layer during healing will result in decreased mechanical strength at the transition interface, with an overall lower degree of motor function compared with that of normal tissue [3–6]. Therefore, promoting a suitable structure for the mineralized bone and fibrocartilage layers is crucial to promote tendon bone healing, although repairing the damaged tendon-to-bone junction may have even greater clinical importance [7,8].

The advances in bone tissue engineering technology have provided promising solutions for the repair of tendon-bone interface injuries. Titanium alloy is the most commonly utilized implant material in orthopedics due to its exceptional physical and chemical properties, including high strength and corrosion resistance [9,10]. Three-dimensional (3D) printing technology allows the preparation of titanium scaffolds through personalized bionic structural bone tissue engineering, which can accurately match bone structures for the treatment of orthopedic diseases [11,12]. The 3D printed titanium alloy microporous scaffolds prepared by electron beam melting (EBM) technology exhibit better mechanical properties, and the microporous structure can increase the contact area between the scaffold and bone, and improve the bone integration ability of the implant [13].

The microporous structured scaffolds can carry hydrogel mixed with growth factors [14,15]. The temperature sensitive collagen hydrogel used in this study was in liquid form at 4 °C and transformed into colloidal state at 37 °C, which made it more convenient to transport

* Corresponding author.
E-mail address: hlf@jlu.edu.cn (L. Huang).

https://doi.org/10.1016/j.mtbio.2025.101549
Received 28 May 2024; Received in revised form 28 January 2025; Accepted 3 February 2025
Available online 4 February 2025
2590-0064/© 2025 The Authors. Published by Elsevier Ltd. This is an open access article under the CC BY-NC-ND license (http://creativecommons.org/licenses/by-nc-nd/4.0/).

growth factors. Growth factors can be transported as a liquid, can be injected into porous scaffolds, and then transformed into the colloidal state at 37 °C, where the colloid degrades at a specific rate. Growth factors are then slowly and continuously released, thus constructing a stable and sustained slow-release system of localized growth factors. The titanium scaffold implantation site is continuously stimulated by growth factors, resulting in more adequate tissue growth between the implant and bone interface and a more stable bone healing interface [16–19].

Transforming growth factor-β (TGF-β) is a growth factor with multiple regulatory functions. TGF-β acts on the tetrameric receptor complex to transduce signals to the classical Smad-dependent signaling pathway and to the non-classical Smad-non-dependent signaling pathway (i.e., p38 MAPK) to regulate stem cell differentiation during skeletal development, bone formation, and bone homeostasis. The Smad and p38 MAPK signaling pathways converge on transcription factors such as Runt-related transcription factor 2 (RUNX2) that promote osteogenic differentiation and differentiation of BMSCs in chondrocytes [20–24]. Among members of the TGF-β family, TGF-β3 regulates the cartilage, bone, tendon, and ligament regeneration process, as well as extracellular matrix secretion and reduction of scar formation in tissue regeneration process; TGF-β3, therefore, serves as a growth factor that promotes tendon/ligament-to-bone healing [25,26].

In this study, we constructed a 3D-printed titanium alloy microporous scaffold filled with TGF-β3 as a "bioactive complex". We verified that TGF-β3 stored in the composite structure can undergo slow and sustained release at the injured site. This improved biological activity of the 3D printed titanium alloy microporous scaffold is conducive to adhesion, proliferation, and differentiation of BMSCs. *In vivo*, the system provided sustained-release of active substances (i.e., TGF-β3) at the injured site, thus promoting the repair of the fibrocartilage layer and the mineralized bone layer at the interface between the ligament and bone (Scheme 1). Hard tissue sections showed that the new bone, ligament, and titanium alloy scaffold system formed a closely integrated whole, and the composite system provided attachment points for ligament growth. In addition, the biomechanical strength of the tendon interface was improved to some extent. The complex effectively promoted long-term tendon/ligament-to-bone healing, providing a theoretical basis for implant design in patients with clinical injuries at the tendon/ligament-to-bone healing site.

2. Materials and methods

2.1. Preparation of 3D printed porous titanium alloy scaffolds

Previous studies have shown that microporous titanium scaffolds with a pore size of 500 μm and 70 % porosity exhibit stronger mechanical properties and better ability to promote bone growth in the micropores of scaffold micropores [19,27,28]. We prepared microporous Ti6Al4V scaffolds with a pore diameter of 500 μm, a porosity of 70 %, and a strut size of 300 μm using the EBM method. Disc-shaped microporous scaffolds (φ10 mm × L3 mm) were used for *in vitro* cell experiments, and column-shaped microporous scaffolds (φ4 mm × L8 mm) were used for *in vivo* animal experiments. Based on the modelling data of the above two scaffolds, model files were designed to perform operations in an EBM instrument (EOS M280, Germany). First, porous scaffolds were prepared by melting Ti6Al4V (TLS, Germany; sphere with a diameter of 45–55 μm) powder layer by layer. After cooling and curing, the samples were removed and sequentially washed in acetone solution, ethanol solution, and deionized water for 60 min, repeating the process three times. The scaffolds were then autoclaved at 121 °C for 20 min and dried in a constant temperature oven at 60 °C. Finally, the dried porous titanium alloy scaffolds were irradiated under ultraviolet light for 60 min.

2.2. Preparation of the 3D-Ti6Al4V/collagen hydrogel/TGF-β3 composite system

Based on previous studies [19,27,29], temperature-sensitive collagen hydrogel was formulated as type I collagen (0.3 % type I collagen; Nitta Gelatin, Osaka, Japan), a 10x culture concentrate, and a reconstitution buffer, which were mixed homogeneously in the ratio of 8:1:1 in a sterile operating table in a 4 °C environment. TGF-β3

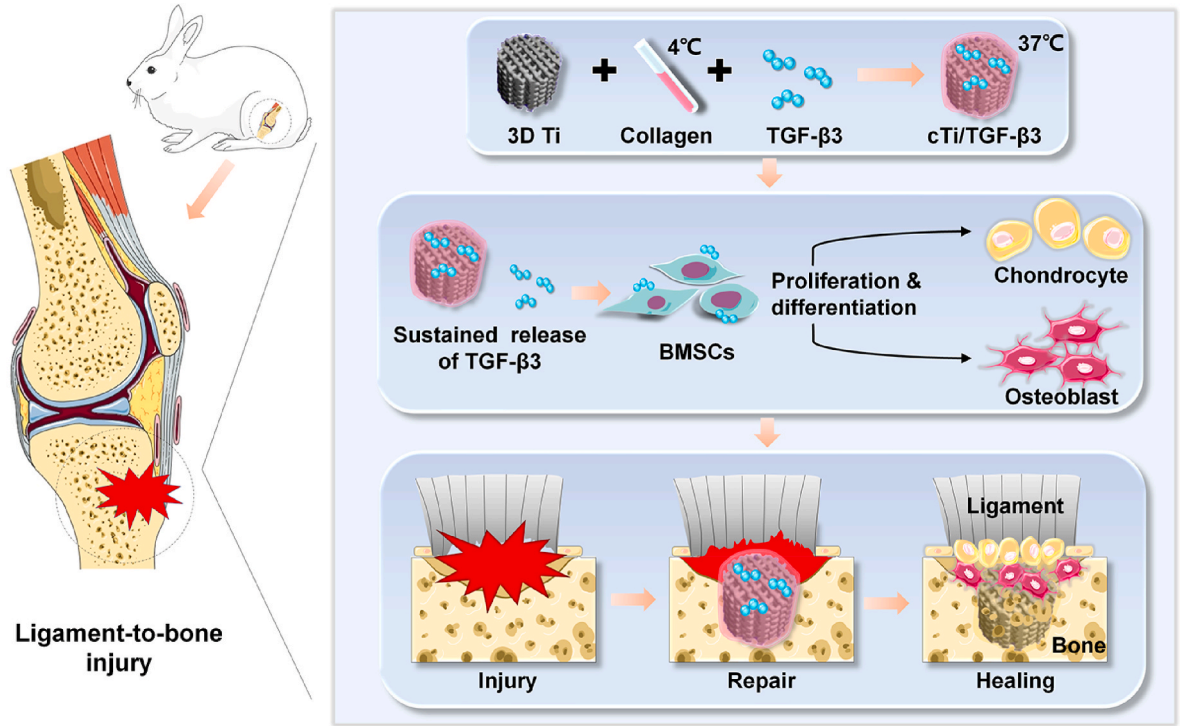

Scheme. 1. Schematic illustration of the promotion of ligament-to-bone interface healing by sustained release of TGF-β3 in this study.

(PeProTech, USA) powder was dissolved in PBS (PBS; Solarbio, Beijing) containing 5 % alginate according to the manufacturer's instructions and then diluted in a solution that could be stored for a prolonged period. Subsequently, TGF-β3 was added to collagen hydrogel at 4 °C with physical mixing and 300 μL of the mixed collagen hydrogel was filled with 3D printed titanium alloy microporous scaffolds. Finally, the titanium scaffolds were placed in 48-well plates and then placed in a cell culture incubator at 37 °C for 30 min.

2.3. Characterization of the material of the composite system

The microstructure of the 3D-Ti6Al4V/collagen hydrogel/TGF-β3 preparation (lyophilized and sprayed with gold) was observed by scanning electron microscopy (SEM; JSM 6700, JEOL, Japan). The surface element distribution of the composite system was analyzed by energy-dispersive X-ray spectroscopy (EDS). The X-ray signal emitted from the sample is collected by an EDS detector, and the signal is converted into an EDS energy spectrum, which is displayed and analyzed by software. The crystal structure of collagen hydrogel coating was characterized by X-ray diffraction (XRD; Rigaku, Japan). Fourier transform infrared spectroscopy (FTIR; Nexus-670, USA) analyzes functional groups in biological coatings.

2.4. TGF-β3 release and hydrogel degradation rate in vitro

Release of TGF-β3 in a temperature-sensitive collagen hydrogel at various time points was determined using an enzyme-linked immunosorbent assay (ELISA). In preliminary experiments, we determined that the optimal concentration of TGF-β3 for cell growth in collagen hydrogel was 100 ng/mL (Fig. S1), the *in vivo* concentration used was 10 μg/mL [30]. TGF-β3 was mixed in collagen hydrogel at a concentration of 100 ng/mL in a 4 °C environment and subsequently transferred to a cell incubator at 37 °C for 30 min to form a complex gel state. First, TGF-β3 was mixed in collagen hydrogel at a concentration of 100 ng/mL in a 4 °C environment and subsequently transferred to a 37°C-cell culture incubator for 30 min to form a gel state complex. Next, 1 mL of the gel state complex was pipetted into a centrifuge tube containing 2 mL of PBS and was subsequently placed in a cell incubator at 37 °C. We collected 2 mL of PBS at different time points (i.e., 12 h, 1 day, 3 days, 5 days, 7 days, 10 days, 14 days, and 21 days) and the collected samples were stored at −20 °C. Finally, the amount of TGF-β3 released at each time point was detected using an ELISA kit (Bioss, Beijing, China) and the absorbance was measured at OD450 (BioTek Instruments, USA). Data were collected and a standard curve was generated based on the standard concentration of the TGF-β3. The amount of TGF-β3 released at the different time point samples was calculated using the standard curve, and an *in vitro* slow-release curve of TGF-β3 was plotted. In order to determine the degradation rate of collagen hydrogel, we conducted experiments at different time points (i.e., 12 h, 1 day, 3 days, 5 days, 7 days, 10 days, 14 days, and 21 days). The degradation rate of hydrogel was calculated by weighing the remaining weight of hydrogel.

2.5. In vitro cell experiments

2.5.1. Cell culture

BMSCs were obtained from the femurs of New Zealand white female rabbits (4 weeks old) and cultured in low-glucose medium (Gibco, USA) supplemented with 10 % (v/v) fetal bovine serum (Gibco, USA) and 1 % (v/v) penicillin/streptomycin (Gibco, USA). BMSCs were incubated at 37 °C temperature under 5 % CO_2 air and the medium was changed every 2–3 days, when the BMSCs reached 80–90 % confluence, the BMSCs were detached from the dishes with 0.25 % trypsin/EDTA (Gibco, USA) and passaged. After incubation and passaging up to the third generation, the BMSCs were used for cytotoxicity, osteogenic differentiation, and chondrogenic differentiation assays. For osteogenic induction, the following were added to the cell culture medium: dexamethasone (100 nmol/L), β-phosphoglycerol (10 mmol/L), and ascorbic acid (50 μmol/L). For chondrogenic induction, the following were added to the cell culture medium: dexamethasone (100 nmol/L), sodium pyruvate (1 mmol/L), Insulin-Transferrin-Selenium (10 mmol/L), ascorbic acid (75 μmol/L), and proline (1 mmol/L).

2.5.2. Biocompatibility of composite system

2.5.2.1. Cytotoxicity assay. Cell experiments were divided into three groups, untreated 3D printed titanium microporous scaffolds (eTi), composite collagen-filled 3D-printed titanium microporous scaffolds (cTi), and collagen-loaded TGF-β3-filled 3D-printed titanium microporous scaffolds (cTi/TGF-β3). Cell activity, adhesion, and proliferation were detected using the Live/Dead staining assay (BestBio, Shanghai, China) and the Cell Counting kit-8 (CCK-8) assay (Bioss, Beijing, China). For the Live/Dead staining assay, cell viability was assessed on days 1, 3, and 7 using the Calcein-AM/PI Double Staining. Three experimental scaffold treatments (i.e., eTi, cTi, and cTi/TGF-β3) were added to 48-well plates containing basal low-glycemic medium, respectively, and BMSCs were inoculated in 48-well plates at 5.0×10^3 cells/well and were incubated in a 37 °C cell culture incubator. After discarding the supernatant, cells were washed twice with prewarmed PBS at 37 °C to remove residual esterase activity. Next, 500 μL of Calcein-AM staining working solution was added to each well and incubated at 37 °C in a cell culture incubator protected from light for 20 min. Cells were washed twice with PBS before the addition of 500 μL of PI staining working solution to each well. The dishes were incubated for 5 min at 37 °C in a light-protected cell culture incubator. The cells were then washed twice with PBS before being observed and photographed with a fluorescence microscope in a light-protected environment.

For the CCK-8 assay, first a blank control group without scaffold was set up and the three experimental scaffold treatments, eTi, cTi, and cTi/TGF-β3 were added to 12 well plates, respectively, containing low-glycemic basic medium. Cells with good growth status of P3 generation were inoculated in 12-well plates at 2.0×10^4 cells/well, and were placed in a 37 °C cell culture incubator. The assay was performed at three time points: on days 1, 3, and 7. In each well, 100 μL of CCK-8 reagent was added and gently mixed with the culture medium before incubation in a cell culture chamber at 37 °C for 2 h. Next, 100 μL of each well was added to a 96-well plate and the OD value at 450 nm was detected using a fully automated enzyme labeling instrument.

2.5.2.2. Cytomorphological assay. The distribution of the microfilament cytoskeleton and the nuclear position of the BMSCs were observed using phalloidin/DAPI staining (Yeasen Biotech, Shanghai, China). The three experimental scaffold treatments eTi, cTi, and cTi/TGF-β3 were added to 48-well plates, and the BMSCs were inoculated in 48-well plates at 5.0×10^3/well, and then placed in a 37 °C cell culture incubator. Phalloidin/DAPI staining assay was performed on day 7. The supernatant was discarded, and the cells were washed twice with pre-warmed PBS at 37 °C. The cells were then fixed with a 4 % formaldehyde solution for 15 min at room temperature and washed three times with PBS. Next, cells were permeabilized with a 0.5 % Triton X-100 solution for 5 min and washed three times with PBS, before the addition of 500 μL of the FITC-conjugated phalloidin working solution to each well. The plate was then incubated for 30 min at room temperature, protected from light, and washed three times with PBS. The nuclei were stained with 500 μL DAPI solution, protected from light, and incubated for 30 s. The plate was immediately observed and photographed with a fluorescence microscope.

2.5.3. Osteogenic differentiation of BMSCs

The study consisted of three experimental scaffold treatment groups: eTi, cTi and cTi/TGF-β3 groups, extracts of these groups were inoculated into 24-well plates precoated with 0.1 % gelatin followed by the

addition of low-glycemic base medium. Furthermore, the BMSCs were inoculated into 24-well plates at 1.0×10^4 cells/well and were placed in the cell culture incubator at 37 °C. Once cell confluence reached 60%–70 %, the complete medium in the wells was carefully aspirated and osteogenic-induced differentiation medium obtained from BMSCs supernatants was added to the 24-well plates. Changes in culture medium were performed every 3 days and Alizarin Red S (1 %, pH = 4.2, Solarbio, Beijing, China) staining was performed on days 7 and 14. The osteogenic induction differentiation medium was aspirated and rinsed twice with deionized water. Next, 1 mL of 4 % neutral formaldehyde solution was added to each well and left to fix for 30 min at room temperature. The neutral formaldehyde solution was then carefully aspirated, and the wells were rinsed twice with deionized water. Subsequently, each well was stained with 1 mL of Alizarin Red S staining solution for 5 min. Thereafter, the Alizarin Red S staining solution was aspirated, and the wells were rinsed three times with deionized water. The osteogenic staining effect was observed under the microscope and photographed.

2.5.4. Chondrogenic differentiation of BMSCs

Extracts from the three experimental groups (eTi, cTi, and cTi/TGF-β3) were added to 24-well plates with low-glycemic base medium. Furthermore, the BMSCs were inoculated in 24-well plates at 1.0×10^4/well and placed in a cell culture incubator at 37 °C. Once cell confluence reached 60%–70 %, the medium was replaced with chondrogenic-induced differentiation medium. The culture medium was changed every three days. On day 14, Alcian Blue (Solarbio, Beijing, China) and Safranin O (Solarbio, Beijing, China) staining were performed. Chondrogenic induction differentiation was removed from the 24-well plates and rinsed twice with PBS. Next, 1 mL of 4 % neutral formaldehyde solution was added to each well and fixed for 30 min at room temperature, the neutral formaldehyde solution was aspirated and rinsed twice with PBS. Finally, each well was stained with 1 mL of Alcian Blue solution for 10 min, the Alcian Blue staining solution was removed, and the plate was rinsed three times with PBS. The 24-well plate was observed and photographed under a microscope. The method of Safranin O staining was the same as that of Alcian Blue staining.

2.5.5. Gene and protein expression of BMSCs

Reverse transcription quantitative polymerase chain reaction (RT-qPCR) was used to detect changes in gene expression of BMSCs from the eTi, cTi, and cTi/TGF-β3 scaffold treatment groups associated with osteogenic differentiation and chondrogenic differentiation ability. The gene expression of RUNX2, bone morphogenetic protein 2 (BMP-2), and type II collagen (COL2) was detected. Primer sequences used are listed in Table 1. Osteogenic-induced differentiation of BMSCs was detected by RUNX2 and BMP-2 gene expression, while chondrogenic-induced differentiation of BMSCs was detected by COL2 expression. The three scaffolds these treatment groups (i.e., eTi, cTi, and cTi/TGF-β3) were added to 6-well plates containing basal medium, and then the BMSCs were inoculated in 6-well plates at 2.0×10^4 cells/well and placed in the cell culture incubator at 37 °C. The osteogenic differentiation steps were the same as those described in section 2.5.3, and the chondrogenic differentiation steps were the same as those described in section 2.5.4. Total RNA was extracted on day 14, followed by cDNA synthesis by reverse transcription. mRNA expression levels were determined using a quantitative real-time qPCR system (Bio-Rad, USA). All samples were standardized using GAPDH as an internal reference primer and calculated using the $2^{-\Delta\Delta Ct}$ method.

Table 1
Primers for RT-qPCR.

Gene	Forward primer	Reverse primer
GAPDH	GAGCACCAGAGGAGGACGA	TGGGATGGAAACTGTGAAGAG
RUNX2	TCAGGCATGTCCCTCGGTAT	TGGCAGGTAGGTATGGTAGTGG
BMP-2	CGTGAGGATTAGCAGGTCTTTG	AGGCGTTTCCGCTGTTTG
COL2	AACACTGCCAACGTCCAGAT	CTGCAGCACGGTATAGGTGA

Immunofluorescence staining was used to detect changes in protein expression associated with osteogenic differentiation and chondrogenic differentiation ability of BMSCs in the eTi, cTi and cTi/TGF-β3 scaffold-treated groups. The osteogenic differentiation steps were the same as those described in section 2.5.3, and the chondrogenic differentiation steps were the same as those described in section 2.5.4. BMSCs were stained with the osteogenic marker polyclonal anti-BMP-2 overnight. After washing, the cells were further stained with Alexa Fluor® 488 secondary antibody, rhodamine-phalloidin, and DAPI, then imaged using the confocal microscope. For protein detection of chondrogenic differentiation ability, BMSCs were stained with the cartilage marker COL2, with specific immunofluorescence staining methods as above.

2.6. In vivo animal experiments

2.6.1. Animal models

All animal experiments were approved by the Jilin University Animal Care and Use Ethics Committee, and all operating procedures were performed in compliance with National Research Council's Guide for the Care and Use of Laboratory Animals. New Zealand white rabbits (male, 6 months old, 3.5 ± 0.5 kg) were randomly divided into three treatment groups: the eTi, cTi, and cTi/TGF-β3 scaffold groups (n = 9 per group). The study established a model to reconstruct the tendon-bone interface from the patellar ligament to the tibial stop of the rabbit knee joint. The surgical site was the right patellar ligament, which was gradually exposed under strict aseptic operation after appropriate anesthesia and disinfection. The patellar ligament was separated from a portion of the tibial stop at an obtuse angle. A 4-mm diameter drill bit was used to create a hole at the point of separation. The stent was then placed perpendicularly at the separation point in each animal in each group, with the free patellar ligament. The incision was closed in layers and antibiotics were administered intramuscularly for 3 days after surgery. Tissues from repaired ligament and bone sites were collected for analysis at 6 and 12 weeks after surgery.

2.6.2. Micro-CT assay

Bone growth in porous racks was evaluated by micro-CT. The bone samples were scanned at 48 kV voltage, 200 μA current, and 18 μm image pixels to obtain a 3D visual reconstruction of the scanned images. The images were then analyzed using a bone analyzer. In the micro-CT analysis, the area where the stent was located was selected. Finally, various parameters were measured from the collected images, including bone volume fraction (BV/TV), trabecular arthritis (Tb.Th), and trabecular separation (Tb.SP), trabecular number (Tb.N).

2.6.3. Histological evaluation

Tibia samples with patellar ligament were collected and the samples were fixed with 4 % paraformaldehyde solution. The fixed samples were then dehydrated with ethanol in a gradient gradually increasing from low to high concentrations, and to achieve transparency samples were submerged in a 1:1 mixture of anhydrous ethanol and xylene for 30 min and then in xylene for 20 min. The samples were then embedded in paraffin. Samples were cut to a thickness of 30 μm for hematoxylin-eosin (H&E) and Masson staining along the longitudinal axis of scaffolds using a hard tissue slicer. From the H&E and Masson stained sections, tissue morphology was observed using digital microscopy to analyze the healing of the tendon-bone union sites at the scaffold, tendon, and bone junctions.

In order to observe the chondrogenesis at the tendon bone site in the animal study, we performed Safranin O-fast green staining and Alcian blue staining on the sections. The collected bone tissue was fixed in 4 % paraformaldehyde, and then after sufficient decalcification, the scaffolds were removed and the bone tissue was embedded and sectioned. Sections were deparaffinized to water, stained first with fast green staining

and then with Safranin O staining. After dehydration and clear processing, the sections were sealed with neutral gum, microscopically observed and photographed. For Alcian blue staining, the sections were dewaxed to water, alcian acidifying solution was applied for acidification treatment, the tissue sections were placed in 1 % Alcian blue staining solution, followed by nuclear solid red re-staining, transparent treatment with anhydrous ethanol, then sealed with neutral gum, and finally observed under microscope.

2.6.4. Mechanical tensile test and mechanical push-out test

Mechanical experiments were used to assess the strength of the titanium alloy scaffold in relation to the tendon and the new bone. The proximal tibial sample was secured to the machine at both ends and kept vertical. The maximum tensile force for the separation of the implant from the tendon tissue was recorded using a hydraulic testing machine. The sample was placed on the plate and kept perpendicular to the plate, and the maximum thrust to separate the implant from bone tissue was recorded by applying longitudinal pressure at a rate of 1 mm/min using the hydraulic testing machine.

2.6.5. Immunohistochemistry

Rabbit tibial and patellar ligament samples were obtained at 6 and 12 weeks and fixed in 4 % paraformaldehyde. After sufficient decalcification, the scaffolds were removed and bone tissues were sectioned. The tissue sections were then processed for antigenic restoration and nonspecific binding sites were blocked using bovine serum proteins. Specific primary antibodies against osteogenic markers BMP-2 and antibodies against chondrogenic markers COL2 were added and incubated overnight at 4 °C. The samples were then washed, and the corresponding secondary antibody was added. Finally, the samples were dehydrated and blocked, and then observed and photographed under a microscope.

2.7. Statistical analysis

All experimental data were expressed as mean ± standard deviation. Data from multiple experimental groups were analyzed using one-way ANOVA and independent sample *t*-test, and statistically analyzed using GraphPad Prism v.8.0. $p < 0.05$ was considered statistically significant.

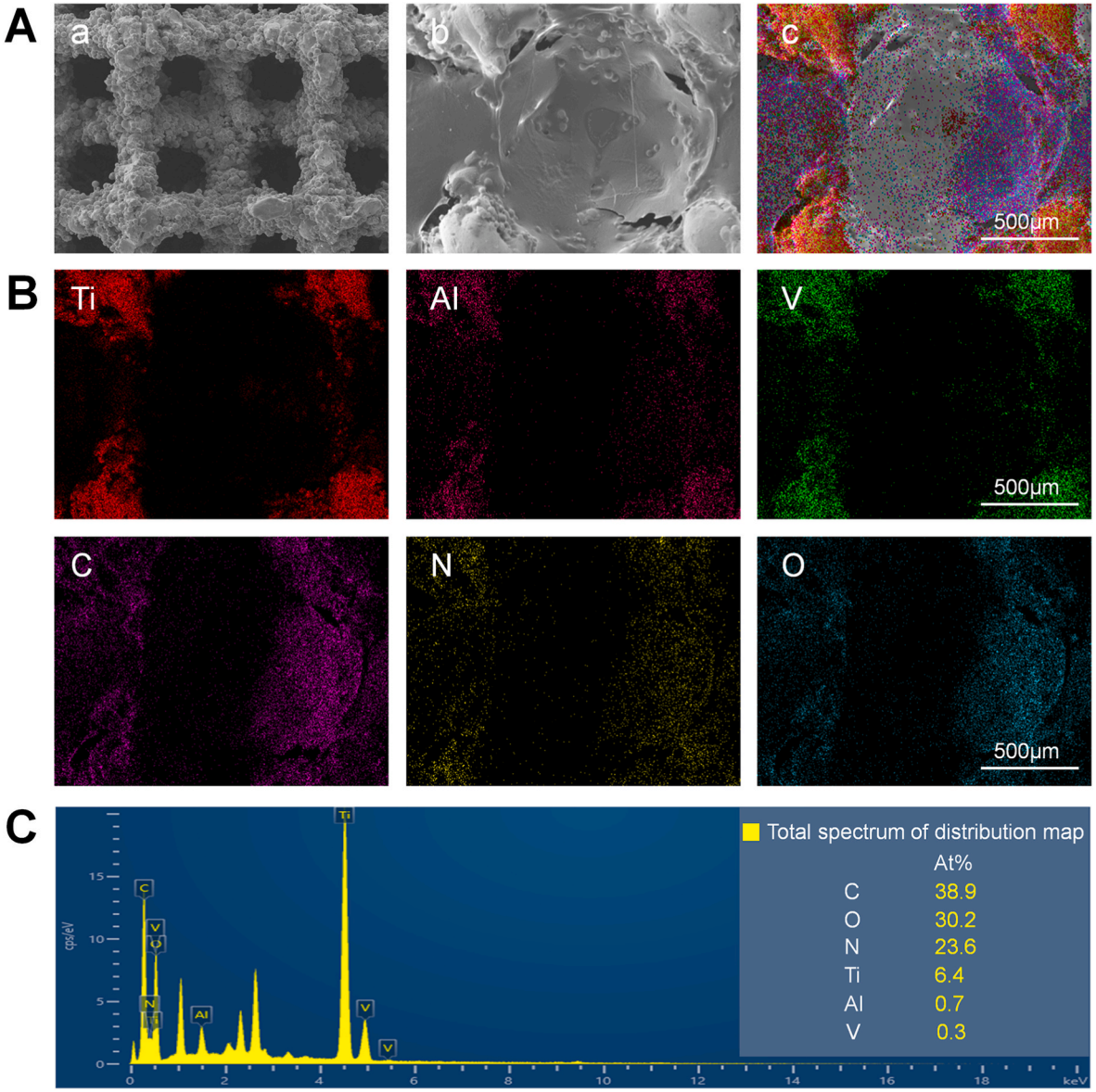

Fig. 1. (A) SEM images of eTi and cTi/TGF-β3 (scale bar = 500 μm); (B) Elemental mapping of cTi/TGF-β3 (scale bar = 500 μm); (C) EDS elemental analysis of cTi/TGF-β3.

3. Results

3.1. Preparation and material characterization of composite scaffolds

The 3D printed titanium alloy microporous scaffolds, disc-shaped microporous scaffolds (φ10 mm × L3 mm), and column-shaped microporous scaffolds (φ4 mm × L8 mm) were prepared using the EBM method (Fig. S2A). The center of the cylindrical scaffold was a 2-mm diameter hollow pore structure, which served to better fix the free ligament tissue and fill the 3D-printed titanium alloy microporous scaffold with temperature-sensitive collagen hydrogel at 4 °C (Fig. S2B). The collagen hydrogel was liquid at a temperature of 4 °C but after exposure to a temperature of 37 °C for 30 min, the collagen hydrogel solidified (Figs. S2C and D). The surface morphology and characteristics of the scaffolds were observed by SEM, and the scaffolds had a porosity of 70 % and a pore diameter of 500 μm (Fig. 1A(a)). Furthermore, the collagen hydrogel uniformly filled the direct microporous structure (Fig. 1A(b)). Elemental mapping (Fig. 1B) and EDS elemental analysis (Fig. 1C) showed the presence of C, N, and O, which confirmed the homogeneous distribution of collagen hydrogel and that of growth factors throughout the composite scaffold. A composite system of 3D printed titanium alloy microporous scaffold filled with collagen hydrogel loaded with TGF-β3 was successfully constructed.

From the XRD analysis, it can also be seen (Fig. S3) that the positions of the diffraction peaks in the XRD spectra of the collagen hydrogel/TGF-β3 group are consistent with those of the collagen hydrogel group, which indicates that the addition of TGF-β3 did not change the crystalline form of the temperature-sensitive collagen, which may be due to

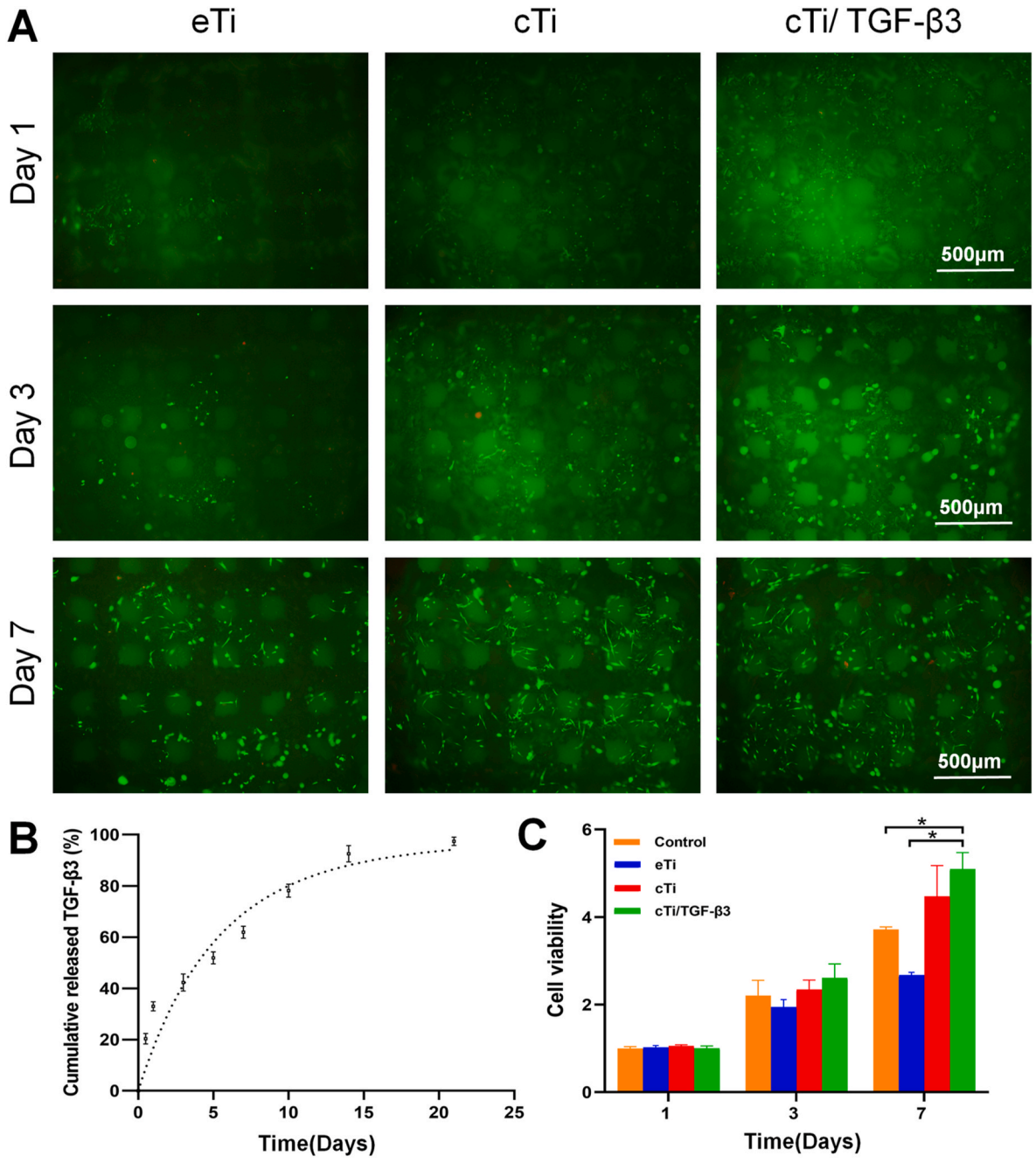

Fig. 2. (A) Live/Dead cell staining of BMSCs at days 1, 3, and 7 (scale bar = 500 μm); (B) Cumulative release of TGF-β3 in collagen hydrogel; (C) Cell viability of BMSCs on different groups for 1, 3, and 7 days (CCK-8) (n = 3, *p < 0.05).

the consistency of the crystalline form of the TGF-β3 and the type I collagen, which is a protein, and it is advantageous for the utilization of the collagen hydrogel-loaded TGF-β3 for the modification and used for subsequent studies is favorable.

Functional groups in collagen hydrogel and collagen hydrogel containing growth factors were analyzed by FTIR (Fig. S4). By comparison between the collagen hydrogel group and the group with added TGF-β3, 3338 cm^{-1} corresponds to O-H or N-H stretching vibrations, commonly originating from hydroxyl and amine groups, which is related to the abundance of amino acids in the protein structure of TGF-β and N-H vibrations in the peptide bonds. 2995 cm^{-1} corresponds to the C-H stretching vibration, which mainly originates from methyl or methylene groups in the amino acid side chains of the TGF-β molecule. 1656 cm^{-1} corresponds to the C=O stretching vibration and is the amide I band, which is commonly found in the infrared spectra of proteins and is mainly associated with the carbonyl vibration in the peptide bond. 1560 cm^{-1} corresponds to the amide II band, reflecting the bending vibration of N-H and the stretching vibration of C-N, which is one of the characteristic peaks of the peptide bond and is directly related to the primary structure of the protein molecule. 1193 cm^{-1} corresponds to the C-O stretching vibration, originating from carboxylic acid groups or post-translational modifications of proteins. It suggests that collagen hydrogel was rich in protein and amino acid structures and that the addition of growth factors does not affect the chemical structure and composition of collagen hydrogel.

3.2. TGF-β3 release assay and the collagen hydrogel degradation rate

ELISA was used to determine the slow-release rate of TGF-β3 in a temperature-sensitive collagen hydrogel. The release of growth factors was more pronounced on day 1 due to the faster degradation rate of the collagen hydrogel (Fig. 2B). The release of TGF-β3 in the complex reached 33.01 % ± 1.76 % on day 1. After an initial burst of TGF-β3 release, 51.91 % ± 2.35 % was released on day 5, and then the rate of the release reached stabilization, and on day 7 it reached 61.96 % ± 2.36 %, and reached 92.56 % ± 3.16 % at day 14, and 97.44 % ± 1.67 % at day 21. TGF-β3 could be released slowly and stably in the collagen hydrogel for more than 21 days. Through the cumulative release of growth factors in a cycle of 21 days, we observed that the collagen hydrogel degraded gradually over time, the degradation was faster in the first 14 days, with the degradation rate of the hydrogel reached 56 % ± 1.39 % by day 7, 89.77 % ± 1.33 % by day 14, and almost complete degradation of the collagen hydrogel by day 21 (Fig. S5). The degradation rate of collagen hydrogel was approximately the same as the cumulative release of growth factors.

3.3. In vitro cell experiments

3.3.1. Cytotoxicity assay

The viability of BMSCs in the three scaffold treatment groups eTi, cTi, and cTi/TGF-β3 was determined by Live/Dead cell staining on days 1, 3, and 7 (Fig. 2A). On day 1, the number of BMSCs in the cTi group and the cTi/TGF-β3 group was higher than in the eTi group, which may be due to the fact that the temperature-sensitive collagen hydrogel filling the pores can provide a good bonding point favorable for cell adhesion of BMSCs. On days 3 and 7, the number of cells in the cTi and cTi/TGF-β3 groups increased faster than in the cTi group, and the scaffold pores in the cTi/TGF-β3 group were filled with cells, suggesting that BMSCs proliferated more rapidly in the collagen hydrogel. The effects of control, eTi, cTi, and cTi/TGF-β3 scaffold groups on cell activity were examined by the CCK-8 assay. On day 1, there was no statistically significant differences in cell activity between the control, eTi, cTi, and cTi/TGF-β3 groups. On day 3, the proliferative capacity of eTi cells was significantly reduced, while that of cTi and cTi/TGF-β3 was elevated, with a more pronounced increase in proliferative capacity in the cTi/TGF-β3 group. On day 7, cell proliferation of the cTi/TGF-β3 group was significantly higher, and was statistically significant when compared with the blank control group and the eTi group ($^*p < 0.05$), whereas the cell proliferation ability of eTi was significantly reduced (Fig. 2C). This may be attributed to eTi providing less space for cell adhesion, which is not conducive to prolonged cell proliferation. Conversely, cell viability was greater in the cTi group than in the blank control group, suggesting that the collagen hydrogel provided additional space for BMSCs to adhere and proliferate and was conducive to improving cell activity. The cTi/TGF-β3 group showed a significant improvement in cell activity on day 7, indicating that TGF-β3 could promote better cell adhesion and proliferation and that the scaffold complex with added TGF-β3 had a more favorable biocompatibility.

3.3.2. Cytomorphological assay

Cytomorphological properties of BMSCs were detected by phalloidin/DAPI staining (Fig. 3). In the eTi group, because of the absence of collagen hydrogel filling in the pores, the BMSCs adhered and grew only on the strut of the titanium scaffold, and the cellular morphology was not fully extended. BMSCs in the cTi and cTi/TGF-β3 scaffold groups filled the titanium scaffolds and pores, which had been fully stretched, the cells were spindle-shaped, and there were more cells in the cTi/TGF-β3 group. The experimental results showed that eTi was not favorable for cell extension, whereas the collagen hydrogel could provide sufficient growth attachment points and a nutrient environment for BMSCs because the collagen hydrogel could sufficiently fill the pores of titanium scaffolds. The cTi and cTi/TGF-β3 groups were more favorable to cell adhesion and extension, and the incorporation of TGF-β3 resulted in stronger BMSCs activity. The good biocompatibility of the cTi and cTi/TGF-β3 groups was revealed by phalloidin/DAPI staining. The addition of collagen hydrogel and TGF-β3 was more favorable for cell adhesion and proliferation.

3.3.3. Osteogenic differentiation of BMSCs

Osteogenic capacity of eTi, cTi, and cTi/TGF-β3 scaffold groups as shown by Alizarin Red S staining solution (Fig. 4). Alizarin Red S can bind to calcium ions, and was used to stain calcification deposits during osteogenic differentiation of cells. On day 7, a small number of calcium salt particles were found to be deposited in eTi and cTi, while more calcium salt particles were deposited in the cTi/TGF-β3 group. On day 14 of osteogenic differentiation, there was a significant increase in calcium salt particles in the cTi/TGF-β3 group, which were combined to form more calcium nodules. Thus, the cTi/TGF-β3 scaffold group had a more pronounced ability to contribute to osteogenic differentiation.

3.3.4. Chondrogenic differentiation of BMSCs

On day 14 after chondrogenic differentiation, cells were stained for characteristic substances such as polysaccharide components and chondroitin sulfate with Alcian Blue and Safranin O stains to assess the chondrogenic capacity of the three treatment groups: eTi, cTi, and cTi/TGF-β3 (Fig. 5 A). Alcian Blue is a negative staining reagent mainly used for staining polysaccharides such as acid polysaccharides and sulfated polysaccharides, and it is particularly well-suited for the visualization of polysaccharide components within the cartilage matrix. Safranin O is a positive staining reagent that can be observed to stain the nucleus of cells and some positively staining substances, such as chondroitin sulfate in cartilage [31,32]. On Alcian Blue staining, the cells of the eTi group appeared to be stained with a lighter shade of blue compared to those of the cTi and cTi/TGF-β3 groups. In addition, both the eTi and cTi groups exhibited stem cell morphology characterized by a long shuttle shape. In contrast, cells in the cTi/TGF-β3 group were clustered, with blue dye filling the area between these clusters. Furthermore, more mucopolysaccharide material was stained blue within the observed area, resulting in a darker shade of blue in the cTi/TGF-β3 group. Safranin O staining revealed that the eTi group had minimal red color throughout the field of view, whereas the cTi group had more red areas than the eTi group. The cTi/TGF-β3 group had the highest number of red areas throughout

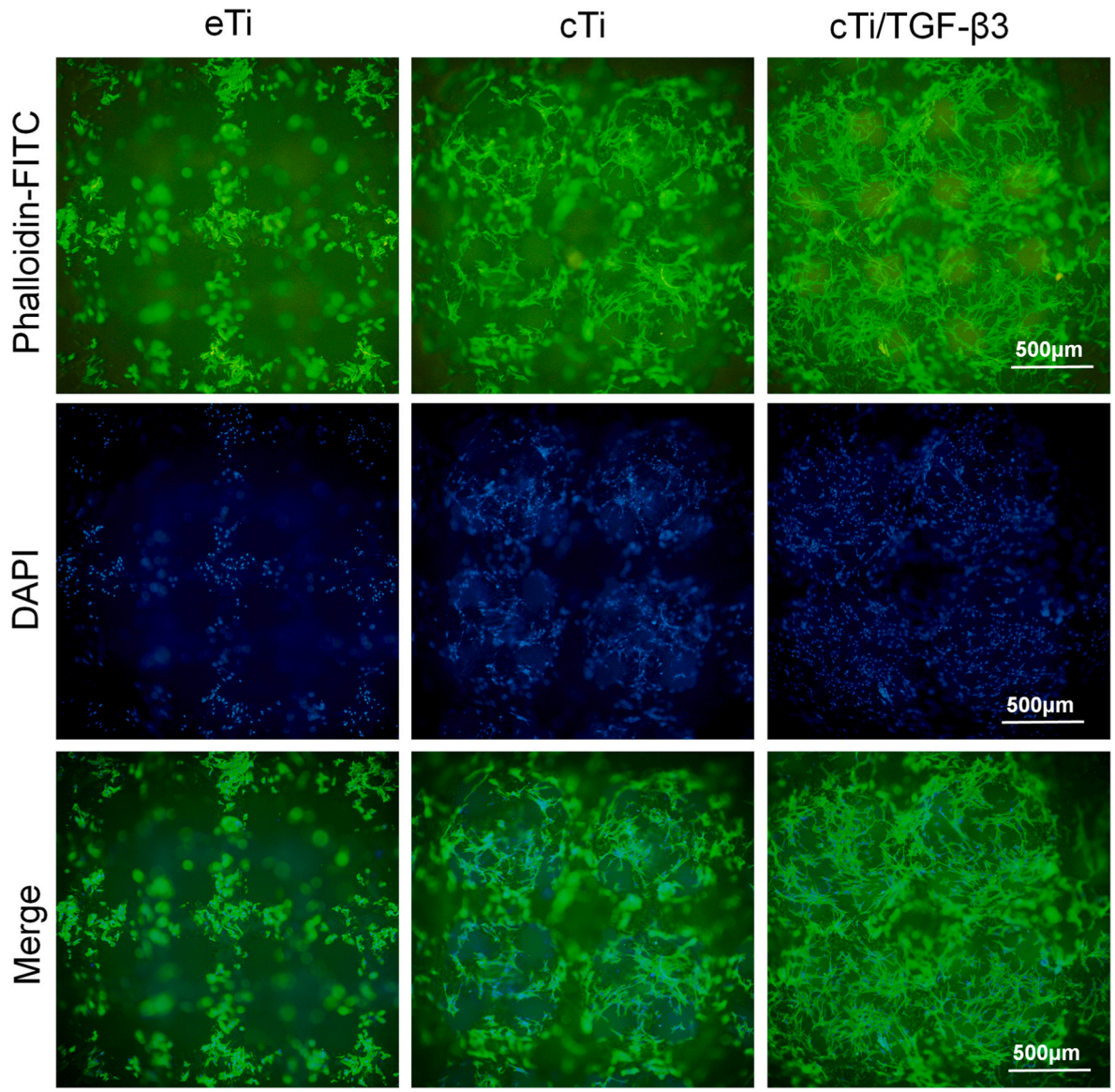

Fig. 3. Phalloidin/DAPI staining of BMSCs at 7 days (scale bar = 500 μm).

the field of view, indicating that the cells in this group secreted more chondroitin sulfate, which combined with the Safranin O staining solution to produce a red color. Alcian Blue staining and Safranin O staining revealed that the cTi/TGF-β3 group had a greater capacity for chondrogenic differentiation.

3.3.5. *Gene and protein expression of BMSCs*

The gene expression following treatment with the three scaffold groups eTi, cTi, and cTi/TGF-β3 was detected by RT-qPCR. As shown in Fig. 5B, RUNX2, a key initiator gene of osteogenic differentiation, increased 3.77 ± 0.32-fold in the cTi/TGF-β3 group compared to eTi, increased 2.53 ± 0.34-fold compared to cTi. The osteogenic gene BMP-2 expression in the cTi/TGF-β3 group increased 5.44 ± 0.60-fold compared with eTi, increased 4.52 ± 0.65-fold compared with cTi. The expression of the chondrogenic gene COL2 in the cTi/TGF-β3 group increased 3.10 ± 0.47-fold compared to eTi, and increased 2.93 ± 0.48-fold compared to cTi. The results of gene expression suggest that the cTi/TGF-β3 group has a greater ability to improve bone and cartilage.

To confirm the role of cTi/TGF-β3 in inducing osteogenesis and chondrogenesis in BMSCs, release medium from different groups was collected and co-cultured with BMSCs at the same seeding density and culture conditions. After 14 days of culture, the expression of osteogenesis-associated protein BMP-2 and chondrogenesis-associated protein COL2 were detected by immunofluorescence. As shown in Fig. 6, after 14 days, BMSCs showed protein expression of both BMP-2 and COL2, and the cTi/TGF-β3 group exhibited relatively high BMP-2 expression and COL2 expression (green fluorescence) relative to the other two groups. The results suggest that cTi/TGF-β3 promotes cellular osteogenic and chondrogenic differentiation compared to other groups.

3.4. *In vivo animal experiments*

3.4.1. *Micro-CT analysis*

To investigate the effect of local growth factor release on tendon bone healing, eTi, cTi and cTi/TGF-β3 were implanted into the tendon-bone injury at the site of the patellar ligament in rabbits. Bone regeneration in each group was observed and quantified by micro-CT after 6 and 12 weeks of implantation. 3D reconstructed micro-CT images showed that the new bone mass in the cTi/TGF-β3 group was higher than that in the other two groups at week 6 and week 12 (Fig. 7A). In contrast, the cTi group was also significantly more numerous than the eTi group, but less than the cTi/TGF-β3 group. This indicates that both

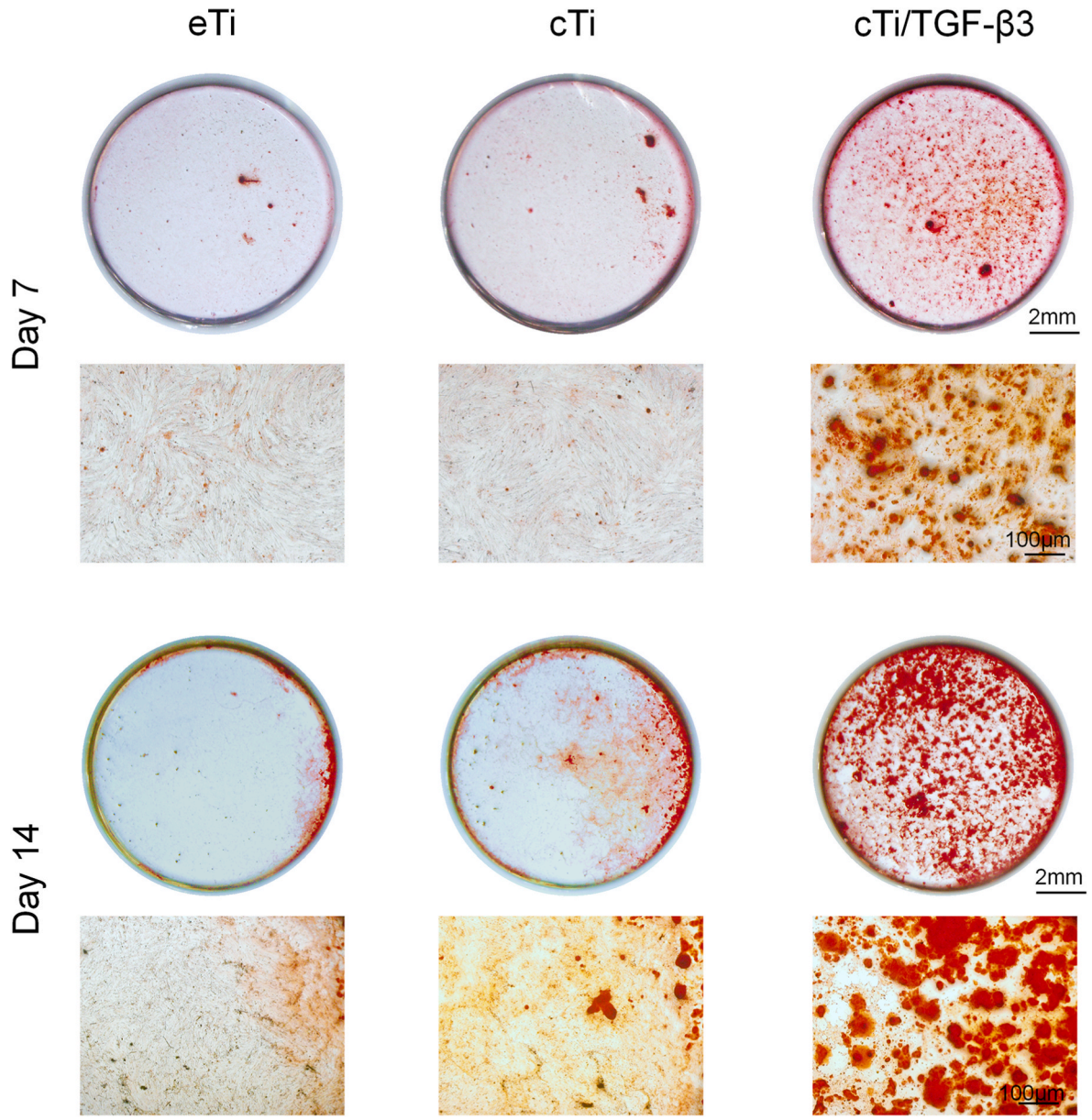

Fig. 4. Alizarin Red S staining of BMSCs cultured on day 7 and 14 (scale bar = 2 mm and 100 μm). (For interpretation of the references to color in this figure legend, the reader is referred to the Web version of this article.)

type I collagen hydrogel and TGF-β3 can promote new bone formation, which may be due to the fact that type I collagen hydrogel provides attachment points for cell adhesion and proliferation. Type I collagen, as an important component of bone, also has a certain promoting effect on bone regeneration. Most importantly, type I collagen hydrogel can also support TGF-β3 to achieve the role of slow-release growth factor, which can continue to release TGF-β3 at the site of tendon bone injury, thereby effectively promoting bone regeneration in the long term. Quantitative parameters of bone in each group were analyzed, and the values of BV/TV, Tb.Th and Tb.N in cTi/TGF-β3 group were significantly higher than those in other groups, and Tb.Sp was the lowest (Fig. 7B–E). These results indicate that TGF-β3 supported by Type I collagen hydrogel has excellent effect on promoting bone regeneration, and can promote bone integration of titanium scaffolds in bone defects.

3.4.2. *Histological evaluation*

A reconstruction model of the ligament-to-bone interface from the patellar ligament to the tibia was constructed in the rabbit knee. The animal experimental modeling protocol is illustrated in Fig. S6 H&E and Masson staining of hard tissue sections (Fig. 8A and B) was examined to detect healing at the ligament-bone union site at the ligament-bone junction. In the H&E-stained sections (Fig. 8A), at week 6, only a small amount of bone tissue was attached around the scaffold and only a small amount of irregular fibrous scar tissue was present in the eTi and cTi groups, whereas in the cTi/TGF-β3 group, a large amount of ligamentous tissue could be observed wrapped around the scaffold and the ligamentous tissue was tightly connected to the new bone tissue. At week 12, the eTi group exhibited a short, disorganized ligament fiber with large gaps between them, appearing as like scar tissue leading to ligament repair. In contrast, the cTi group did not show any fibrous arrangement, but a large amount of ligament tissue was generated. Conversely, in the 12-week cTi/TGF-β3 group, significantly thick and organized ligament tissue was observed and bone tissue was also present between the ligament and scaffold, with ligament and bone tissue tightly bound to the scaffold. In the Masson-stained sections (Fig. 8B), at week 6, there were fewer ligament fibers in the eTi and cTi groups, the fibers

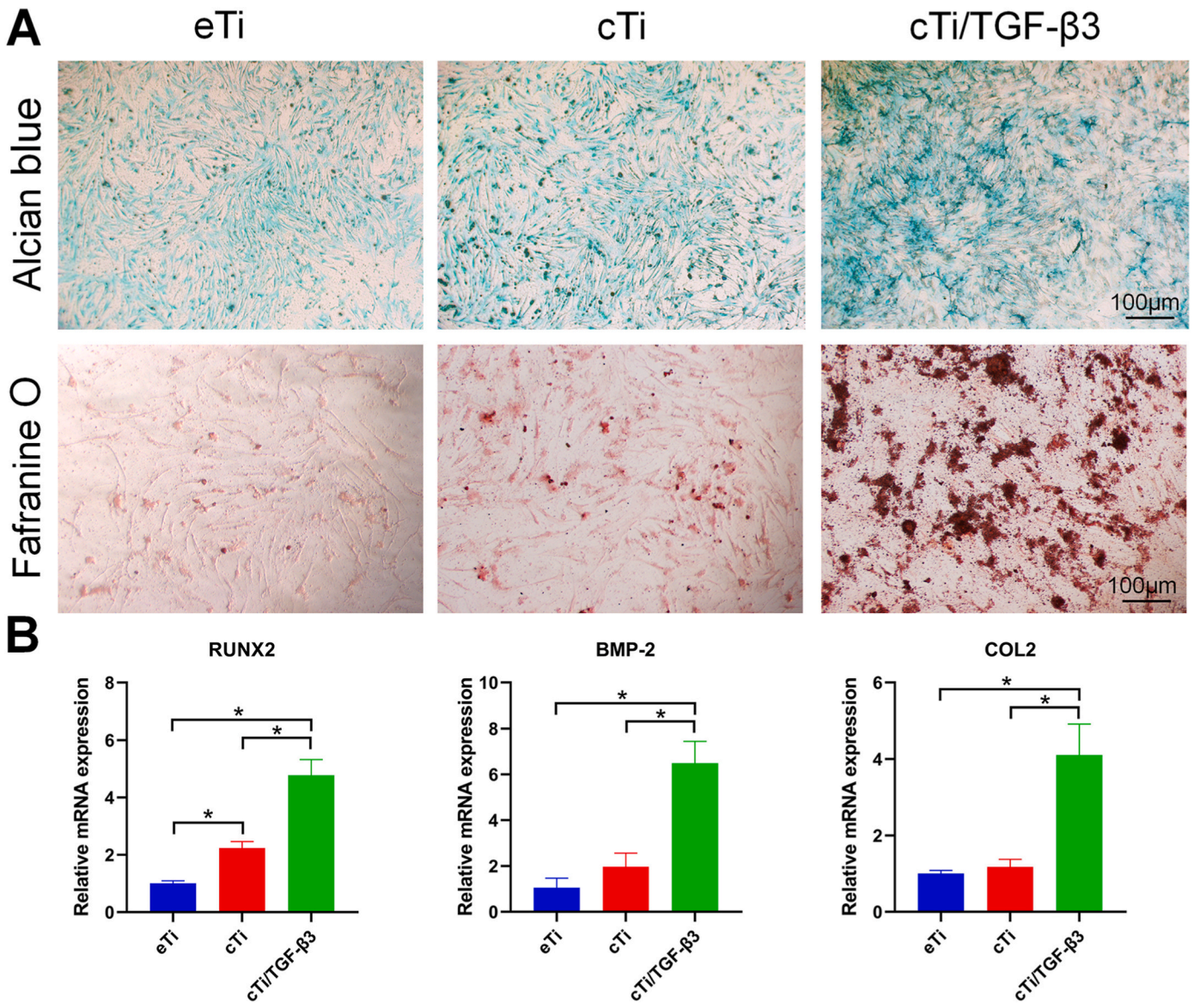

Fig. 5. (A) Chondrogenic differentiation of BMSCs induced by scaffold treatment in eTi, cTi, and cTi/TGF-β3 groups at day 14; stained with Alcian Blue and Safranin O (scale bar = 100 μm); (B) Relative mRNA expression of osteogenesis genes RUNX2, BMP-2 and chondrogenic genes COL2 in BMSCs (n = 3, *p < 0.05). (For interpretation of the references to color in this figure legend, the reader is referred to the Web version of this article.)

were irregularly arranged, and only a small amount of bone tissue was generated around the titanium scaffold. In the cTi/TGF-β3 group, regularly arranged ligament tissue was observed wrapping around the scaffolds and a clear area of attachment was visible between ligament tissue and neoplastic bone tissue. At week 12, the fiber content of the ligament in eTi remained low and only a small amount of bone tissue was attached to the titanium scaffold. In the cTi group, although a large amount of tissue was generated from the newborn muscle fiber, it was irregularly arranged. The section of cTi/TGF-β3 group at 12 weeks showed that the titanium scaffold was attached to the newly formed bone tissue and a distinct and regular transition area was evident between the newly formed ligamentous fibrous tissue and the newly formed bone. This may represent the cartilaginous transition area between the ligament and the bone, which facilitates the tight integration of the newly formed ligament fibrous tissue, the newly formed bone tissue, and the titanium scaffold. The results of hard tissue sections showed that the cTi/TGF-β3 group had formed stable titanium scaffolds with the surrounding bone and ligaments, which could more effectively promote tissue growth at the ligament/tendon-bone tissue junction.

Safranin O-Fast Green Staining and Alcian Blue Staining were performed to evaluate cartilage regeneration at the ligament-bone interface. In Safranin O-Fast Green Staining, cartilage tissues appeared red or orange-red, bone tissues appeared green or blue, and muscle and collagen fibers appeared gray-green. Compared with the eTi and cTi groups, cTi/TGF-β3 group had more areas of red color (Fig. S7A), indicating increased chondrocyte differentiation. In Alcian Blue staining, the endoacidic mucopolysaccharides of cartilage tissues reacted with Alcian Blue staining solution to become blue. cTi/TGF-β3 group had more blue areas than the other two groups (Fig. S7B). In conclusion, cTi/TGF-β3 promotes cartilage formation in the tendon-bone union.

3.4.3. *Mechanical tensile test and mechanical push-out test*

The strength of the bond between the scaffold, the new bone, and the ligament tissue was evaluated using mechanical tensile and push-out tests. During the tensile tests, all groups showed rupture of the ligament attachment point at the critical point of the tensile force with no pull-out of the titanium stent. In the maximal tensile force experiment (Fig. 8C), at weeks 6 and 12, the maximum tensile tolerance in the cTi/

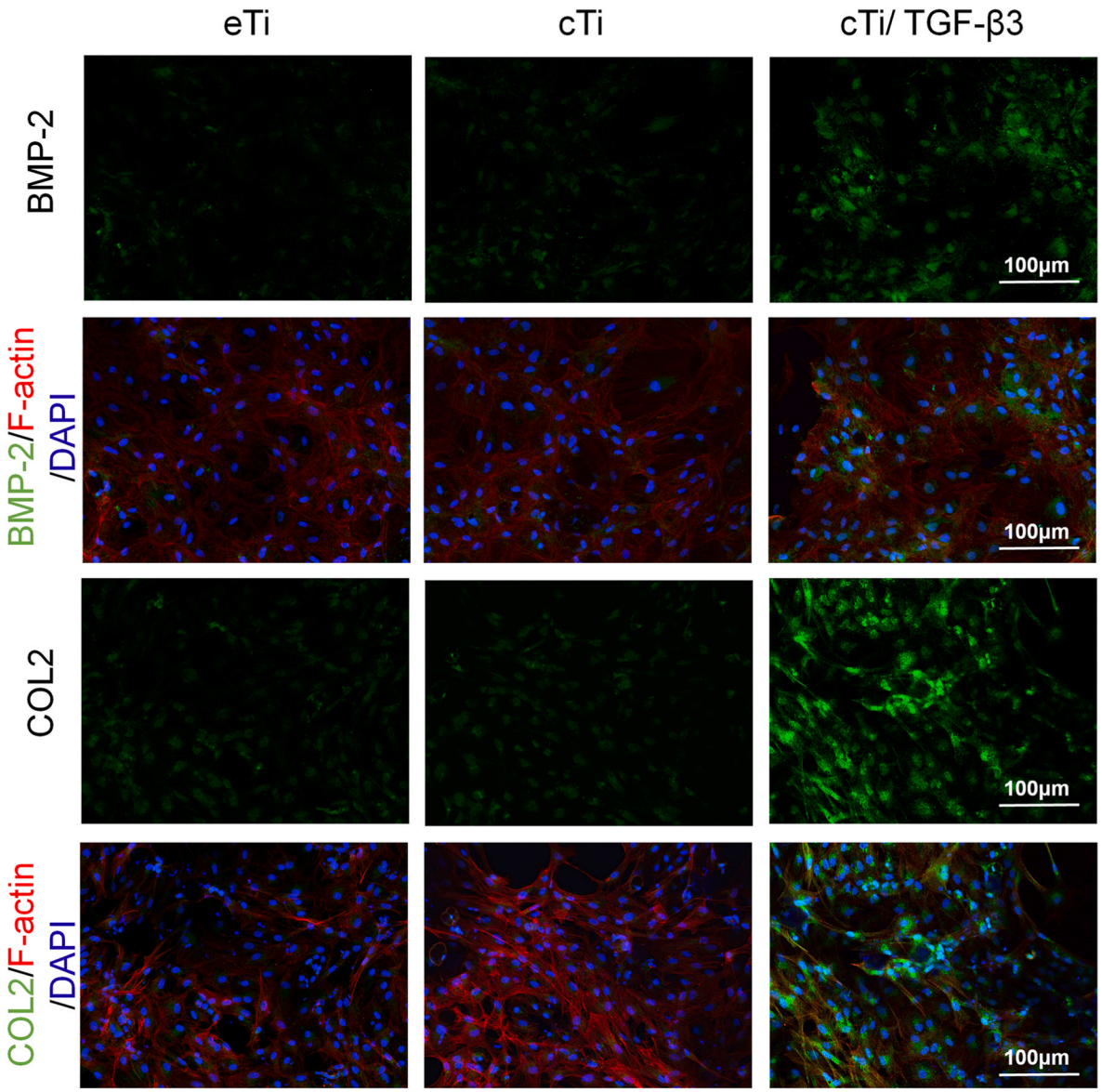

Fig. 6. Immunofluorescence staining of the osteogenic marker BMP-2 (green: BMP-2; red: F-actin; blue: DAPI) and the chondrogenic marker COL2 (green: COL2; red: F-actin; blue: DAPI) was confocal imaged after 14 days of osteogenic and chondrogenic induced differentiation of BMSCs. (For interpretation of the references to color in this figure legend, the reader is referred to the Web version of this article.)

TGF-β3 scaffold group increased by 14.88 ± 1.83 N and 41.40 ± 2.12 N compared to the eTi group and increased by 9.01 ± 2.11 N and 29.70 ± 1.98 N compared to the cTi. In the maximal push-out force test (Fig. 8D), at weeks 6 and 12, the cTi/TGF-β3 scaffold group was more strongly bound to bone tissue, and the maximum push-out tolerance increased by 159.3 ± 14.06 N and 199.9 ± 14.09 N compared to the eTi group, and by 101.9 ± 10.46 N and 78.98 ± 17.90 N compared to the cTi group. Thus, at weeks 6 and 12, the cTi group and the cTi/TGF-β3 group demonstrated superior tensile strength and pushout resistance compared to the eTi group, and also the cTi/TGF-β3 group exhibited higher binding strength than the other 2 types of scaffolds. Overall, the results indicate that the cTi/TGF-β3 group achieved greater bone growth in titanium alloy scaffolds and enhanced the integration of the scaffolds with the bone, resulting in enhanced push-out force resistance. Additionally, cTi/TGF-β3 treatment improved the bonding strength at the scaffold-ligament-bone interface, enabling it to withstand stronger tensile force.

3.4.4. *Immunohistochemistry*

Immunohistochemical staining was used to further investigate bone and cartilage regeneration at the scaffold-ligament-bone interface. Ligament-to-bone tissue was labeled with BMP-2 antibodies to evaluate the formation of new bone and cartilage at the scaffold-bone interface. Positive labeling was indicated by a brownish-yellow color and a rounded or ovoid morphology. Compared with the eTi and cTi groups, the cTi/TGF-β3 scaffold group showed higher expression of BMP-2 expression (Fig. 9A), indicating increased osteoblast differentiation and improved cartilage formation. The cartilage of the sectioned tissue was labeled with the COL2 antibody and exhibited a tan color with round or ovoid morphology. The cTi/TGF-β3 scaffold treatment group presented greater cartilage marker expression than the eTi and cTi groups (Fig. 9B). In summary, cTi/TGF-β3 promoted new bone formation in the mineralized bone layer at the tendon-bone union site and also stimulated regeneration of the fibrocartilage layer.

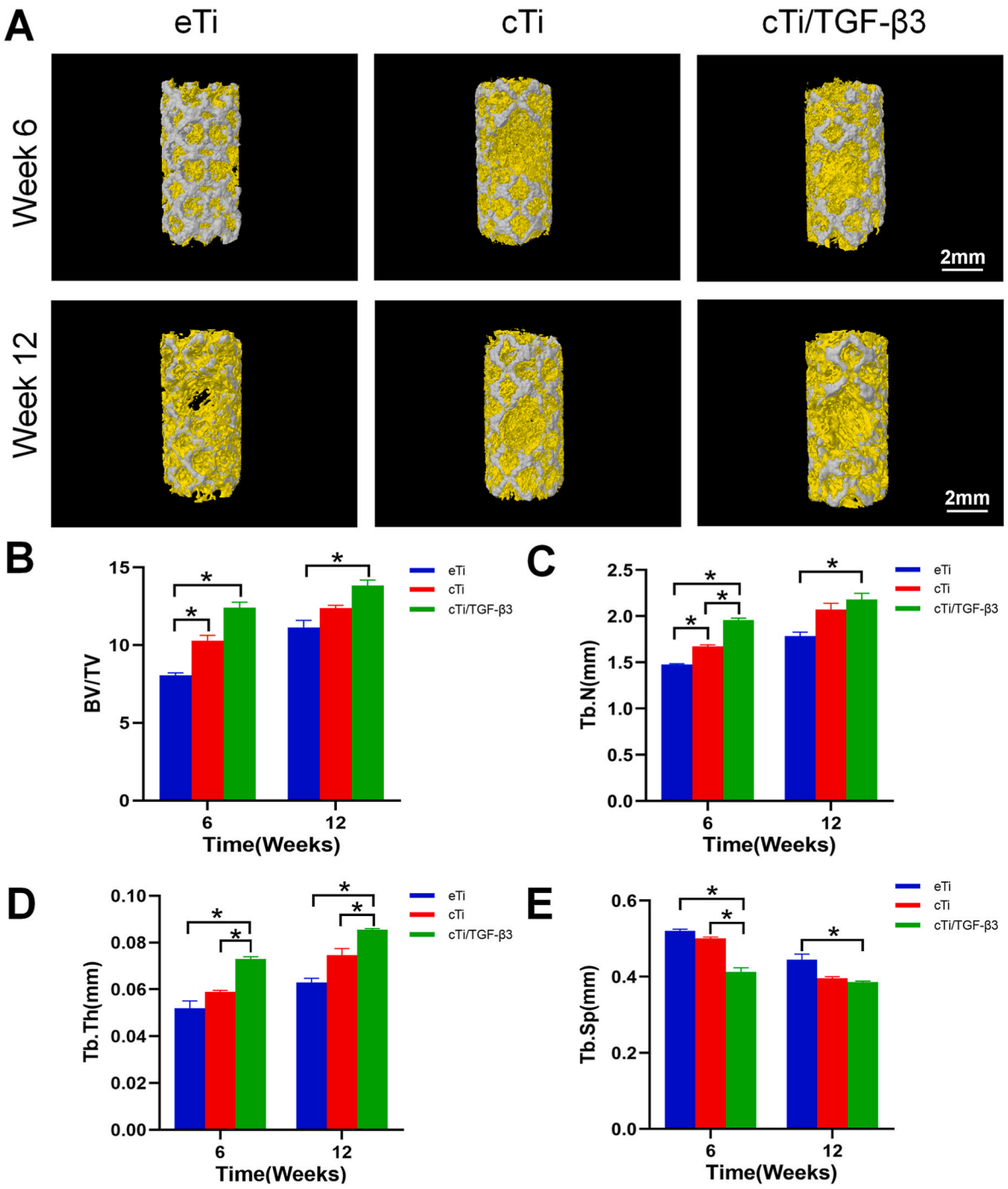

Fig. 7. (A) Micro-CT 3D reconstructed images of eTi, cTi, and cTi/TGF-β3 groups and their quantitative analysis (scale bar = 2 mm); (B) BV/TV, (C) Tb.N, (D) Tb.Th and (E) Tb.Sp (n = 3, *p < 0.05).

4. Discussion

Currently, reconstructive surgery of the tendon/ligament-to-bone interface presents a challenge in orthopedics. This is due to the poor biocompatibility of most implants, which do not integrate well with the surrounding tissues and are often replaced by scar tissue after injury, resulting in frequent failure to form a stable structure after repair of tendon/ligament-to-bone injuries. Furthermore, the use of implants can prolong healing time, causing potential complications such as infection or chronic pain [33–35]. Clinical treatment of orthopedic diseases requires accelerated healing and reduced complications with an accelerated return to normal function [36]. The tendon/ligament-to-bone interface is structurally complex, with a four-layer structure comprising the tendon/ligament, uncalcified fibrocartilage, calcified fibrocartilage, and bone [5,6]. Promoting the healing of the tendon/ligament-to-bone interface is an intensive area of research in bone tissue engineering. Surgical repair of the damaged tendon-bone union site and post-operative functional recovery are urgent clinical concerns.

With the development of bone tissue engineering, prosthetic implants, autologous tendon grafts, and local loading of growth factors have been extensively studied [37]. Titanium alloys are widely used in clinical treatment and bone tissue engineering research due to their bio-inertness and excellent mechanical properties. The application of 3D printing has been used to customize the shape of the prosthesis to fit the

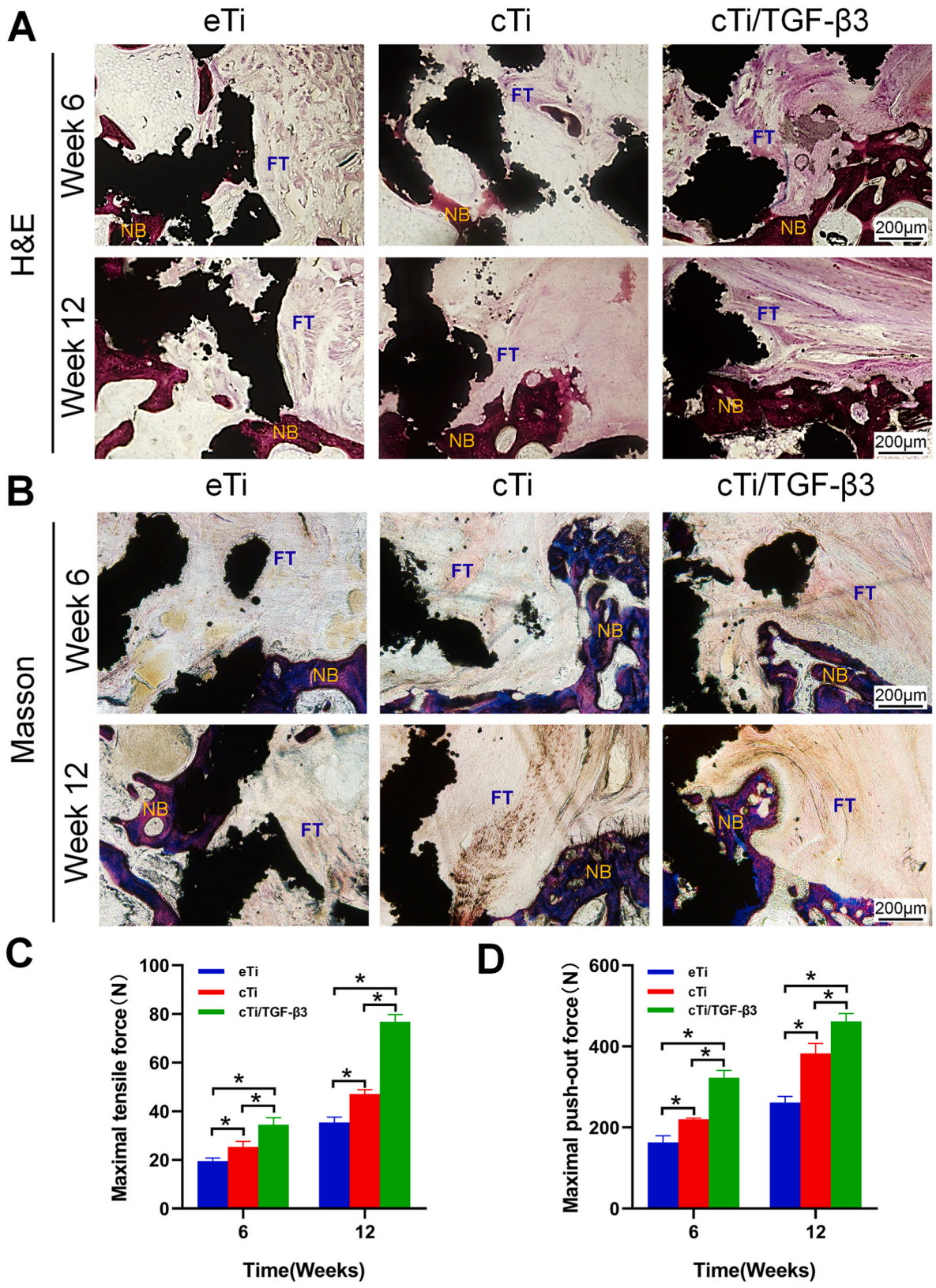

Fig. 8. Hard tissue sections of the eTi, cTi, and cTi/TGF-β3 scaffold treatment groups at weeks 6 and 12. (A) H&E staining (the light red area labeled FT indicates tendon tissue, the dark red area labeled NB indicates new bone tissue, and the black areas are titanium scaffolds, scale bar = 200 μm) and (B) Masson staining (the light red area labeled FT indicates ligament tissue, the blue area labeled NB indicates new bone tissue, and the black areas are titanium scaffolds, scale bar = 200 μm). (C) Maximum tensile force and (D) maximum pushout force at weeks 6 and 12 for the eTi, cTi, and cTi/TGF-β3 groups (n = 3, *p < 0.05). (For interpretation of the references to color in this figure legend, the reader is referred to the Web version of this article.)

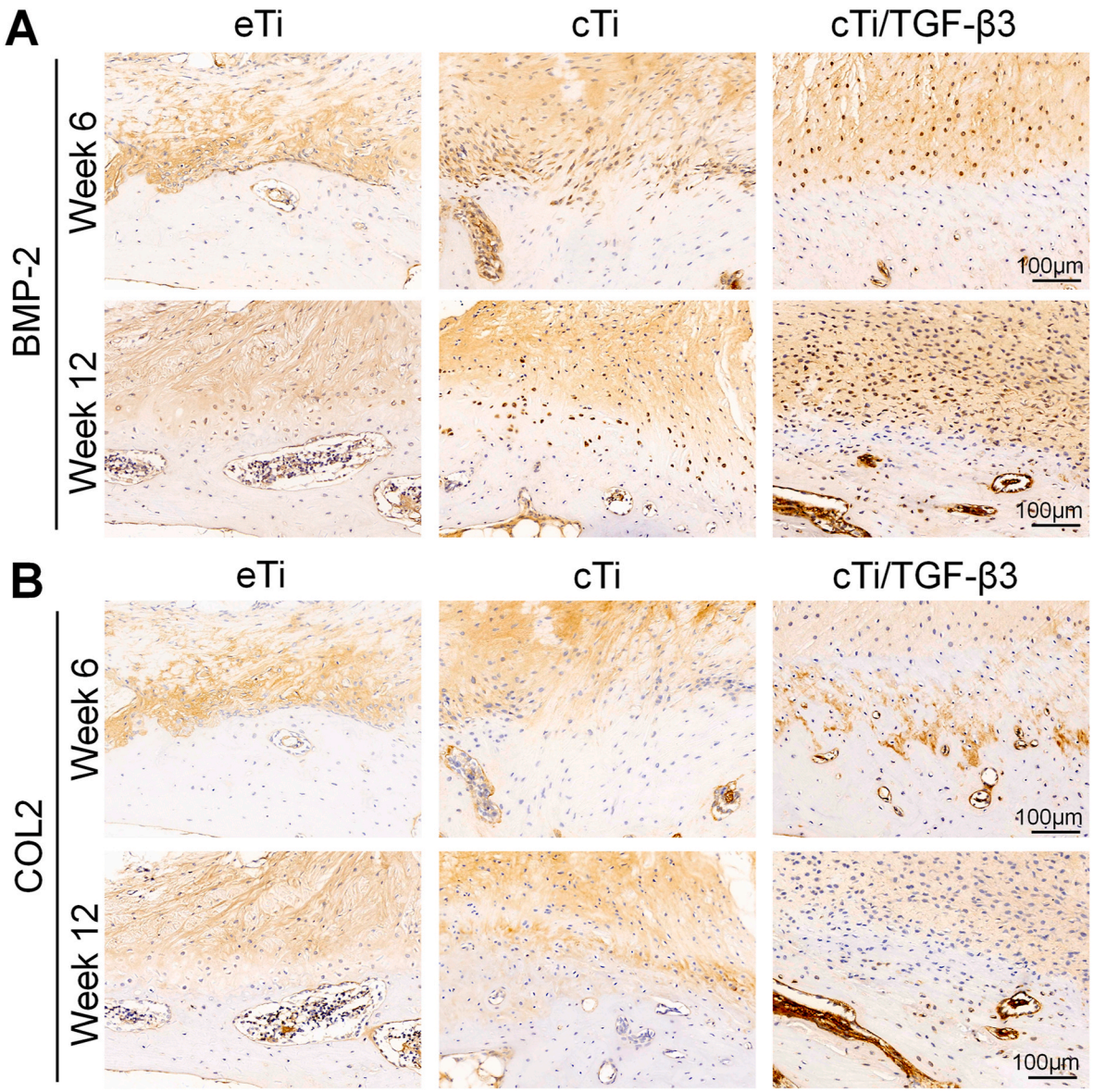

Fig. 9. Immunohistochemical staining using (A) BMP-2 and (B) COL2 antibodies in the eTi, cTi, and cTi/TGF-β3 scaffold treatment groups (scale bar = 100 μm).

injury site and control porosity and pore size to facilitate bone tissue growth [16–19].

A growing number of studies has shown that BMSCs play an important role in tendon/ligament-to-bone healing. BMSCs have multidirectional differentiation potential and can differentiate into osteoblasts, chondrocytes, and adipocytes [38,39]; thus, participating in the formation and repair of neoplastic tissue during the tendon/ligament-to-bone healing. Meanwhile, BMSCs can secrete a variety of growth factors, such as angiogenic factor (VEGF) and BMP, to promote vascularization and osteoblast proliferation [40–42]. BMSCs also induce anti-inflammatory and immunomodulatory effects [43–46], which reduce inflammatory damage during the healing process and favor tendon bone healing and repair. Interestingly, macrophages and BMSCs interact with each other, and the macrophage phenotype may provide a new approach to the treatment of tendon bone injuries [47].

Growth factor applications may lead to new breakthroughs in the treatment of orthopedic diseases [48,49]. Advancements in current research suggest that biologics may play a significant role, with a variety of pharmacologic interventions demonstrating their strong capacity to promote fracture healing [50,51]. TGF-β3 is a growth factor with multiple regulatory functions, including the regeneration process of cartilage, bone, tendons, and ligaments, as well as modulating the secretion of components of extracellular matrix, which reduces scarring during tissue regeneration [20,52,53]. During tendon/ligament-to-bone healing, the TGF-β signaling pathway plays a crucial role in regulating cell proliferation, collagen synthesis, and differentiation of tendon and bone progenitor cells, yielding tendon/ligament-to-bone formation. TGF-β regulates several signaling pathways involved in the promotion of proliferation and differentiation of BMSCs. The Smad signaling pathway is an important signaling pathway active in the skeletal system. TGF-β activates Smad proteins by binding to its receptor, forming the Smad complex in the nucleus, and regulating gene transcription [23]. TGF-β signaling also exhibits crosstalk with several key cytokine signaling pathways, including MAPK, Wnt/β-catenin, Hedgehog, Notch, PI3K/Akt, PTHrP, and FGF, to influence BMSCs proliferation and differentiation to orchestrate osteogenesis, skeletal development, and bone homeostasis [20–25]. Therefore, TGF-β3 is widely used in various studies due to its potent role in promoting growth and development of the skeletal system. A current research objective is focusing on how to incorporate TGF-β3 into implants to enable its continuous stimulation of tissue healing at the site of injury.

In this study examining potential treatment of tendon-bone injuries,

exogenous TGF-β3 was used to promote the repair of internal tissues in the body. In previous experimental studies, we have shown that the temperature-sensitive collagen hydrogel can carry growth factors and completely fill the porous structure of titanium scaffolds [19]. This collagen hydrogel can reach a swelling equilibrium state at 10 h with a swelling rate of up to 110 % [27]. In addition, our data using FTIR analysis revealed the occurrence of vibrational coupling of specific amino acid side chains or peptide groups, the interaction forces between molecules in the collagen hydrogel, and the presence of collagen hydrogel containing growth factors. The collagen hydrogel was confirmed to bind to titanium scaffolds by XRD analysis, and titanium scaffolds modified with collagen and growth factors exhibited a lower contact angle compared with the original 3D printed titanium alloy [29]. Stable bioactive complexes were formed using temperature-sensitive collagen as a carrier for TGF-β3. These complexes were then injected into the pores of 3D-printed titanium alloy microporous scaffolds, which became gelatinous at 37 °C. Our *in vitro* experiments demonstrated that temperature-sensitive collagen sustained the slow release of TGF-β3, inducing osteogenesis and chondrogenesis over an extended time period. Cell-based experiments confirmed the excellent biocompatibility of the cTi/TGF-β3 complex through the CCK-8 cell proliferation assay, Live/Dead cell staining, and phalloidin/DAPI staining. In addition, enhanced osteogenic and chondrogenic differentiation of the cTi/TGF-β3 complex was confirmed by Alizarin Red S staining, Alcian Blue staining, and Safranin O staining. The RT-qPCR results indicated that the composite system upregulated the expression of the RUNX2, BMP-2, and COL2 genes, promoting osteogenic and chondrogenic differentiation of BMSCs. The high expression of RUNX2 in BMSCs plays an important role in the skeletal system [22,54]. Osteoblasts originate primarily from bone marrow mesenchymal stem cells, and their differentiation is regulated mainly by RUNX2. Activation of RUNX2 leads to osteogenic differentiation of bone progenitor cells, resulting in the expression of osteogenesis-specific markers such as BMP-2, increased alkaline phosphatase activity, and increased secretion of bone matrix-associated proteins [6]. BMP-2 is a member of the TGF-β superfamily. It has the ability to induce the directed differentiation and proliferation of undifferentiated mesenchymal stem cells into chondrocytes and osteoblasts. Furthermore, it promotes the differentiation and maturation of osteoblasts, which are involved in the growth, development, and reconstruction of bone and cartilage. This accelerates the repair of bone defects [49]. Chondrocytes produce matrix and fibers (mainly type II collagen), and the high expression of the COL2 gene in tendon bone healing contributes to the promotion of endogenous collagen synthesis, facilitates cartilage repair, and regulates cellular activity [55], which is of positive significance for tendon bone healing and restoration of structural function.

In vivo experiments in our study, through the analysis of hard tissue sections, showed that the cTi/TGF-β3 complex can provide a stable attachment point for the ligament, and the resulting ligament tissue exhibits a more ordered fibrous structure. In addition, the bone tissue grew into the pores of the scaffold, and the ligament, the bone, and the implant formed a stable structure. The tensile force and push-out experiments demonstrated that the composite system could effectively increase mechanical strength so that the ligament-to-bone interface could withstand greater forces. The immunohistochemical results showed that at the site of ligament-to-bone injury, implantation of the scaffold preparation promoted the expression of the relevant markers BMP-2 and COL2. In summary, the composite system of cTi/TGF-β3 effectively promoted bone growth and facilitated the healing of ligament-to-bone injury sites.

Our experimental study showed that the use of collagen hydrogel carrying growth factors yielded a stable complex with the implant and achieved a better therapeutic effect on orthopedic diseases. In particular, an implant featuring sustained slow-release of growth factors developed herein had a more powerful therapeutic ability than different implants without growth factors. However, there are still many limitations and shortcomings in this project. For instance, it remains unclear how the titanium scaffold achieves the optimal shape that matches the injury site and its effect on the local stress distribution and motor function of the limb. Furthermore, there is also the question of the presence of an initial burst of growth factor release from collagen hydrogel, and the various roles *in vivo* should be more extensively investigated.

Meanwhile, it is unclear how TGF-β3 activity maintains its continuous function *in vivo*, particularly in the healing of tendon/ligament-to-bone injury. This process involves multiple types of cells and is influenced by various factors [56,57]. Furthermore, the healing process of ligament/tendon-bone injury is the result of a series of orderly physiological repair processes determined by various cell types under the influence of multiple factors. This process requires the progressive repair of the damaged ligament/tendon-to-bone interface to an ordered four-layer structure comprising tendon/ligament, uncalcified fibrocartilage, calcified fibrocartilage, and bone. These repair mechanisms require further exploration to achieve a better understanding of complete injury healing.

5. Conclusions

This study describes the construction of a composite system consisting of 3D-printed titanium microporous scaffolds filled with temperature-sensitive collagen hydrogel loaded with TGF-β3. The collagen hydrogel showed the ability to carry growth factors, allowing for slow release of TGF-β3 over an extended period of time. We showed that this continuous stimulation promoted tissue repair at the site of ligament/tendon-to-bone injury. The composite system developed in this study effectively promoted bone growth in the scaffold and repaired the bone defect site, but also served as an attachment point for ligament growth, increased cartilage formation, enhanced ligament repair, reduced scar tissue generation, and increased mechanical strength of the ligament/tendon-bone union site. In general, our bioactive composite system can effectively promote bone growth in the site of ligament/tendon-bone injury. This study provides novel ideas for implant design in patients with clinical ligament/tendon-to-bone site injuries.

CRediT authorship contribution statement

Liwei Zhu: Writing – review & editing, Writing – original draft, Methodology, Investigation, Conceptualization. **Yuzhe Liu:** Software, Formal analysis, Data curation. **Yifu Sun:** Writing – original draft, Resources, Conceptualization. **Zhenjia Che:** Resources, Methodology. **Youbin Li:** Writing – original draft, Project administration. **Tengyue Liu:** Validation, Formal analysis. **Xudong Li:** Conceptualization. **Chengzhe Yang:** Writing – original draft. **Lanfeng Huang:** Visualization, Supervision, Resources, Project administration, Funding acquisition, Conceptualization.

Funding

This work was sponsored by Natural Science Foundation of Jilin Province, China (Grant Number YDZJ202401429ZYTS).

Declaration of competing interest

The authors declare that they have no known competing financial interests or personal relationships that could have appeared to influence the work reported in this paper.

Appendix A. Supplementary data

Supplementary data to this article can be found online at https://doi.org/10.1016/j.mtbio.2025.101549.

Data availability

Data will be made available on request.

References

[1] C.L. Zhu, J.C. Qiu, S. Thomopoulos, Y.N. Xia, Augmenting tendon-to-bone repair with functionally graded scaffolds, Adv. Healthcare Mater. 10 (2021) 2002269, https://doi.org/10.1002/adhm.202002269.

[2] G. Nourissat, F. Berenbaum, D. Duprez, Tendon injury: from biology to tendon repair, Nat. Rev. Rheumatol. 11 (2015) 223–233, https://doi.org/10.1038/nrrheum.2015.26.

[3] S. Thomopoulos, W.C. Parks, D.B. Rifkin, K.A. Derwin, Mechanisms of tendon injury and repair, J. Orthop. Res. 33 (2015) 832–839, https://doi.org/10.1002/jor.22806.

[4] D. Docheva, S.A. Müller, M. Majewski, C.H. Evans, Biologics for tendon repair, Adv. Drug Deliv. Rev. 84 (2015) 222–239, https://doi.org/10.1016/j.addr.2014.11.015.

[5] B.B. Rothrauff, R.S. Tuan, Cellular therapy in bone-tendon interface regeneration, Organogenesis 10 (2014) 13–28, https://doi.org/10.4161/org.27404.

[6] I. Calejo, R. Costa-Almeida, M.E. Gomes, Cellular complexity at the interface: challenges in enthesis tissue engineering cell biology and translational medicine, Vol 5, Stem Cell.: Transl. Sci. Therapy 1144 (2019) 71–90, https://doi.org/10.1007/5584_2018_307.

[7] H. Yuk, T. Zhang, S.T. Lin, G.A. Parada, X.H. Zhao, Tough bonding of hydrogels to diverse non-porous surfaces, Nat. Mater. 15 (2016) 190, https://doi.org/10.1038/nmat4463.

[8] X.X. Li, R.Y. Cheng, Z.Y. Sun, W. Su, G.Q. Pan, S. Zhao, J.Z. Zhao, W.G. Cui, Flexible bipolar nanofibrous membranes for improving gradient microstructure in tendon-to-bone healing, Acta Biomater. 61 (2017) 204–216, https://doi.org/10.1016/j.actbio.2017.07.044.

[9] Y.T. Sul, C.B. Johansson, S. Petronis, A. Krozer, Y. Jeong, A. Wennerberg, T. Albrektsson, Characteristics of the surface oxides on turned and electrochemically oxidized pure titanium implants up to dielectric breakdown: the oxide thickness, micropore configurations, surface roughness, crystal structure and chemical composition, Biomaterials 23 (2002) 491–501, https://doi.org/10.1016/s0142-9612(01)00131-4.

[10] M. Geetha, A.K. Singh, R. Asokamani, A.K. Gogia, Ti based biomaterials, the ultimate choice for orthopaedic implants - a review, Prog. Mater. Sci. 54 (2009) 397–425, https://doi.org/10.1016/j.pmatsci.2008.06.004.

[11] M. Mirkhalaf, Y. Men, R. Wang, Y. No, H. Zreiqat, Personalized 3D printed bone scaffolds, A review Acta Biomater 156 (2023) 110–124, https://doi.org/10.1016/j.actbio.2022.04.014.

[12] L. Du, C. Qin, H.J. Zhang, F. Han, J.M. Xue, Y.F. Wang, J.F. Wu, Y. Xiao, Z.G. Huan, C.T. Wu, Multicellular bioprinting of biomimetic inks for tendon-to-bone regeneration, Adv. Sci. 10 (2023), https://doi.org/10.1002/advs.202301309.

[13] A. Palmquist, M. Jolic, E. Hryha, F.A. Shah, Complex geometry and integrated macro-porosity: clinical applications of electron beam melting to fabricate bespoke bone-anchored implants, Acta Biomater. 156 (2023) 125–145, https://doi.org/10.1016/j.actbio.2022.06.002.

[14] A. Zielinska, J. Karczewski, P. Eder, T. Kolanowski, M. Szalata, K. Wielgus, M. Szalata, D. Kim, S.R. Shin, R. Slomski, E.B. Souto, Scaffolds for drug delivery and tissue engineering: the role of genetics, J. Contr. Release 359 (2023) 207–223, https://doi.org/10.1016/j.jconrel.2023.05.042.

[15] Y.B. Li, Y.Z. Liu, R.H. Li, H.T. Bai, Z.Q. Zhu, L.W. Zhu, C.Y. Zhu, Z.J. Che, H. Liu, J. C. Wang, L.F. Huang, Collagen-based biomaterials for bone tissue engineering, Mater. Des. 210 (2021) 110049, https://doi.org/10.1016/j.matdes.2021.110049.

[16] F.Y. Teng, I.C. Tai, M.L. Ho, J.W. Wang, L. Weng, Y.J. Wang, M.W. Wang, C. C. Tseng, Controlled release of BMP-2 from titanium with electrodeposition modification enhancing critical size bone formation Mater, Sci. Eng. C-Mater. Biol. Appl. 105 (2019) 11, https://doi.org/10.1016/j.msec.2019.109879. Article 109879.

[17] Z.Y. Chen, X.C. Yan, S. Yin, L.L. Liu, X. Liu, G.R. Zhao, W.Y. Ma, W.Z. Qi, Z.M. Ren, H.L. Liao, M. Liu, D.Z. Cai, H. Fang, Influence of the pore size and porosity of selective laser melted Ti6Al4V ELI porous scaffold on cell proliferation, osteogenesis and bone ingrowth, Mater. Sci. Eng. C-Mater. Biol. Appl. 106 (2020) 13, https://doi.org/10.1016/j.msec.2019.110289. Article 110289.

[18] B.L. Tao, Y.M. Deng, L.Y. Song, W.W. Ma, Y. Qian, C.C. Lin, Z. Yuan, L. Lu, M. W. Chen, X. Yang, K.Y. Cai, BMP2-loaded titania nanotubes coating with pH-responsive multilayers for bacterial infections inhibition and osteogenic activity improvement, Colloid Surf. B-Biointerfaces 177 (2019) 242–252, https://doi.org/10.1016/j.colsurfb.2019.02.014.

[19] Z.Q. Zhu, X. Li, Y.B. Li, L.W. Zhu, C.Y. Zhu, Z.J. Che, L.F. Huang, Three-dimensionally printed porous biomimetic composite for sustained release of recombinant human bone morphogenetic protein 9 to promote osteointegration, Mater. Des. 208 (2021) 109882, https://doi.org/10.1016/j.matdes.2021.109882.

[20] M. Wu, G. Chen, Y.P. Li, TGF-beta and BMP signaling in osteoblast, skeletal development, and bone formation, homeostasis and disease, Bone Res 4 (2016) 16009, https://doi.org/10.1038/boneres.2016.9.

[21] J.L. Crane, X. Cao, Bone marrow mesenchymal stem cells and TGF-β signaling in bone remodeling, J. Clin. Investig. 124 (2014) 466–472, https://doi.org/10.1172/jci70050.

[22] M.S. Rahman, N. Akhtar, H.M. Jamil, R.S. Banik, S.M. Asaduzzaman, TGF-β/BMP signaling and other molecular events: regulation of osteoblastogenesis and bone formation, Bone Res. 3 (2015) 15005, https://doi.org/10.1038/boneres.2015.5.

[23] M.L. Zou, Z.H. Chen, Y.Y. Teng, S.Y. Liu, Y. Jia, K.W. Zhang, Z.L. Sun, J.J. Wu, Z. D. Yuan, Y. Feng, X. Li, R.S. Xu, F.L. Yuan, The Smad dependent TGF-β and BMP signaling pathway in bone remodeling and therapies, Front. Mol. Biosci. 8 (2021) 593310, https://doi.org/10.3389/fmolb.2021.593310.

[24] K. Luo, Signaling cross talk between TGF-β/Smad and other signaling pathways, Cold Spring Harbor Perspect. Biol. 9 (2017) a022137, https://doi.org/10.1101/cshperspect.a022137.

[25] X.M. Du, L.Y. Cai, J. Xie, X.D. Zhou, The role of TGF-beta3 in cartilage development and osteoarthritis, Bone Res 11 (2023) 2, https://doi.org/10.1038/s41413-022-00239-4.

[26] H. Shen, H. Lin, A.X. Sun, S.J. Song, B. Wang, Y.H. Yang, J.W. Dai, R.S. Tuan, Acceleration of chondrogenic differentiation of human mesenchymal stem cells by sustained growth factor release in 3D graphene oxide incorporated hydrogels, Acta Biomater. 105 (2020) 44–55, 10.10165.actbio.2020.01.048.

[27] Y. Li, Y. Liu, H. Bai, R. Li, J. Shang, Z. Zhu, L. Zhu, C. Zhu, Z. Che, J. Wang, H. Liu, L. Huang, Sustained release of VEGF to promote angiogenesis and osteointegration of three-dimensional printed biomimetic titanium alloy implants, Front. Bioeng. Biotechnol. 9 (2021), https://doi.org/10.3389/fbioe.2021.757767.

[28] A. Arjunan, M. Demetriou, A. Baroutaji, C. Wang, Mechanical performance of highly permeable laser melted Ti6Al4V bone scaffolds, J. Mech. Behav. Biomed. Mater. 102 (2020) 103517, https://doi.org/10.1016/j.jmbbm.2019.103517.

[29] Z.J. Che, Y.F. Sun, W.B. Luo, L.W. Zhu, Y.B. Li, C.Y. Zhu, T.Y. Liu, L.F. Huang, Bifunctionalized hydrogels promote angiogenesis and osseointegration at the interface of three-dimensionally printed porous titanium scaffolds, Mater. Des. 223 (2022) 111118, https://doi.org/10.1016/j.matdes.2022.111118.

[30] Y.H. Deng, A.X. Sun, K.J. Overholt, G.Z. Yu, M.R. Fritch, P.G. Alexander, H. Shen, R.S. Tuan, H. Lin, Enhancing chondrogenesis and mechanical strength retention in physiologically relevant hydrogels with incorporation of hyaluronic acid and direct loading of TGF-β, Acta Biomater. 83 (2019) 167–176, https://doi.org/10.1016/j.actbio.2018.11.022.

[31] L.Y. Cai, Y.J. Cui, D.M. Guo, H. Chen, J.Z. Li, X.D. Zhou, J. Xie, Microenvironmental stiffness directs chondrogenic lineages of stem cells from the human apical papilla via cooperation between ROCK and Smad3 signaling, ACS Biomater. Sci. Eng. 9 (2023) 4831–4845, https://doi.org/10.1021/acsbiomaterials.2c01371.

[32] Z.J. Wang, H.Y. Yang, X. Xu, H.X. Hu, Y.X. Bai, J. Hai, L.M. Cheng, R.R. Zhu, Ion elemental-optimized layered double hydroxide nanoparticles promote chondrogenic differentiation and intervertebral disc regeneration of mesenchymal stem cells through focal adhesion signaling pathway, Bioact. Mater. 22 (2023) 75–90, https://doi.org/10.1016/j.bioactmat.2022.08.023.

[33] T.N. Hissnauer, N. Stiel, K. Babin, M. Rupprecht, M. Hoffmann, J.M. Rueger, R. Stuecker, A.S. Spiro, Bone morphogenetic protein-2 for the treatment of congenital pseudarthrosis of the tibia or persistent tibial nonunion in children and adolescents: a retrospective study with a minimum 2-year follow-up, J. Mater. Sci. Mater. Med. 28 (2017) 8, https://doi.org/10.1007/s10856-017-5868-9. Article 60.

[34] C. von Ruden, M. Morgenstern, C. Hierholzer, S. Hackl, F.L. Gradinger, A. Woltmann, V. Buhren, J. Friederichs, The missing effect of human recombinant Bone Morphogenetic Proteins BMP-2 and BMP-7 in surgical treatment of aseptic forearm nonunion, Injury-Int, J. Care Inj. 47 (2016) 919–924, https://doi.org/10.1016/j.injury.2015.11.038.

[35] P. Annis, D.S. Brodke, W.R. Spiker, M.D. Daubs, B.D. Lawrence, The fate of L5-S1 with low-dose BMP-2 and pelvic fixation, with or without interbody fusion, in adult deformity surgery, Spine 40 (2015) E634–E639, https://doi.org/10.1097/brs.0000000000000867.

[36] J. Goldhahn, W.H. Scheele, B.H. Mitlak, E. Abadie, P. Aspenberg, P. Augat, M. L. Brandi, N. Burlet, A. Chines, P.D. Delmas, I. Dupin-Roger, D. Ethgen, B. Hanson, F. Hartl, J.A. Kanis, R. Kewalramani, A. Laslop, D. Marsh, S. Ormarsdottir, R. Rizzoli, A. Santora, G. Schmidmaier, M. Wagener, J.Y. Reginster, Clinical evaluation of medicinal products for acceleration of fracture healing in patients with osteoporosis, Bone 43 (2008) 343–347, https://doi.org/10.1016/j.bone.2008.04.017.

[37] C.H. Yang, Y.J. Teng, B. Geng, H.F. Xiao, C.S. Chen, R.J. Chen, F. Yang, Y.Y. Xia, Strategies for promoting tendon-bone healing: current status and prospects, Front. Bioeng. Biotechnol. 11 (2023) 1118468, https://doi.org/10.3389/fbioe.2023.1118468.

[38] R. Gadkari, L.Z. Zhao, T. Teklemariam, B.M. Hantash, Human embryonic stem cell derived-mesenchymal stem cells: an alternative mesenchymal stem cell source for regenerative medicine therapy, Regen. Med. 9 (2014) 453–465, https://doi.org/10.2217/rme.14.13.

[39] A. Winter, S. Breit, D. Parsch, K. Benz, E. Steck, H. Hauner, R.M. Weber, V. Ewerbeck, W. Richter, Cartilage-like gene expression in differentiated human stem cell spheroids - a comparison of bone marrow-derived and adipose tissue-derived stromal cells, Arthritis Rheum. 48 (2003) 418–429, https://doi.org/10.1002/art.10767.

[40] N.H. Chi, M.C. Yang, T.W. Chung, J.Y. Chen, N.K. Chou, S.S. Wang, Cardiac repair achieved by bone marrow mesenchymal stem cells/silk fibroin/hyaluronic acid patches in a rat of myocardial infarction model, Biomaterials 33 (2012) 5541–5551, https://doi.org/10.1016/j.biomaterials.2012.04.030.

[41] R.I. Sharma, J.G. Snedeker, Paracrine interactions between mesenchymal stem cells affect substrate driven differentiation toward tendon and bone phenotypes, PLoS One 7 (2012) e31504, https://doi.org/10.1371/journal.pone.0031504.

[42] X.R. Fu, G. Liu, A. Halim, Y. Ju, Q. Luo, G.B. Song, Mesenchymal stem cell migration and tissue repair, Cells 8 (2019) 784, https://doi.org/10.3390/cells8080784.
[43] J.X. Zou, W.A. Yang, W.S. Cui, C.S. Li, C.Y. Ma, X.X. Ji, J.Q. Hong, Z.H. Qu, J. Chen, A. Liu, H.B. Wu, Therapeutic potential and mechanisms of mesenchymal stem cell-derived exosomes as bioactive materials in tendon-bone healing, J. Nanobiotechnol. 21 (2023) 14, https://doi.org/10.1186/s12951-023-01778-6.
[44] J.K. Zhang, H.T. Shi, N. Zhang, L.R. Hu, W. Jing, J. Pan, Interleukin-4-loaded hydrogel scaffold regulates macrophages polarization to promote bone mesenchymal stem cells osteogenic differentiation via TGF-beta 1/Smad pathway for repair of bone defect, Cell Prolif. 53 (2020) e12907, https://doi.org/10.1111/cpr.12907.
[45] Q. Zhao, X.R. Liu, C.Y. Yu, Y. Xiao, Macrophages and bone marrow-derived mesenchymal stem cells work in concert to promote fracture healing: a brief review, DNA Cell Biol. 41 (2022) 276–284, https://doi.org/10.1089/dna.2021.0869.
[46] C. Schlundt, H. Fischer, C.H. Bucher, C. Rendenbach, G.N. Duda, K. Schmidt-Bleek, The multifaceted roles of macrophages in bone regeneration: a story of polarization, activation and time, Acta Biomater. 133 (2021) 46–57, https://doi.org/10.1016/j.actbio.2021.04.052.
[47] Z. Chen, M.C. Jin, H.Y. He, J.B. Dong, J. Li, J.B. Nie, Z.C. Wang, J.T. Xu, F.F. Wu, Mesenchymal stem cells and macrophages and their interactions in tendon-bone healing, J. Orthop. Transl. 39 (2023) 63–73, https://doi.org/10.1016/j.jot.2022.12.005.
[48] Z.J. Che, Y. Song, L.W. Zhu, T.Y. Liu, X.D. Li, L.F. Huang, Emerging roles of growth factors in osteonecrosis of the femoral head, Front. Genet. 13 (2022) 1037190, https://doi.org/10.3389/fgene.2022.1037190.
[49] L. Zhu, Y. Liu, A. Wang, Z. Zhu, Y. Li, C. Zhu, Z. Che, T. Liu, H. Liu, L. Huang, Application of BMP in bone tissue engineering, Front. Bioeng. Biotechnol. 10 (2022), https://doi.org/10.3389/fbioe.2022.810880.
[50] T.A. Einhorn, L.C. Gerstenfeld, Fracture healing: mechanisms and interventions, Nat. Rev. Rheumatol. 11 (2015) 45–54, https://doi.org/10.1038/nrrheum.2014.164.
[51] R.E. Dent-Acosta, N. Storm, R.S. Steiner, J. San Martin, The tactics of modern-day regulatory trials, J Bone Joint Surg Am 94 (Suppl 1) (2012) 39–44, https://doi.org/10.2106/JBJS.L.00194.
[52] K. Miyazawa, M. Shinozaki, T. Hara, T. Furuya, K. Miyazono, Two major Smad pathways in TGF-beta superfamily signalling, Genes Cells 7 (2002) 1191–1204, https://doi.org/10.1046/j.1365-2443.2002.00599.x.
[53] M. Taghavi, A. Parham, A. Raji, The combination of TGF-beta 3 and BMP-6 synergistically promotes the chondrogenic differentiation of equine bone marrow-derived mesenchymal stem cells, Int. J. Pept. Res. Therapeut. 26 (2020) 727–735, https://doi.org/10.1007/s10989-019-09880-w.
[54] S. Vimalraj, B. Arumugam, P.J. Miranda, N. Selvamurugan, Runx2: structure, function, and phosphorylation in osteoblast differentiation, Int. J. Biol. Macromol. 78 (2015) 202–208, https://doi.org/10.1016/j.ijbiomac.2015.04.008.
[55] Y. Liu, G. Dzidotor, T.T. Le, T. Vinikoor, K. Morgan, E.J. Curry, R. Das, A. McClinton, E. Eisenberg, L.N. Apuzzo, K.T.M. Tran, P. Prasad, T.J. Flanagan, S. W. Lee, H.M. Kan, M.T. Chorsi, K.W.H. Lo, C.T. Laurencin, T.D. Nguyen, Exercise-induced piezoelectric stimulation for cartilage regeneration in rabbits, Sci. Transl. Med. 14 (2022) eabi7282, https://doi.org/10.1126/scitranslmed.abi7282.
[56] J. Wang, Y. Zhang, J. Cao, Y. Wang, N. Anwar, Z.H. Zhang, D.M. Zhang, Y.P. Ma, Y. Xiao, L. Xiao, X. Wang, The role of autophagy in bone metabolism and clinical significance, Autophagy 19 (2023) 2409–2427, https://doi.org/10.1080/15548627.2023.2186112.
[57] A.D. Berendsen, B.R. Olsen, Bone development, Bone 80 (2015) 14–18, https://doi.org/10.1016/j.bone.2015.04.035.